Fatigue Behavior of FRP Composites and CNT-Embedded FRP Composites: A Review

Anand Gaurav, Kalyan K. Singh
Department of Mechanical Engineering, Indian School of Mines (ISM), Dhanbad, Jharkhand 826004, India

Composite materials have emerged as an effective substitute for conventional materials in various fields of engineering and structural science. For replacement of regular metals, composites, especially fiber-reinforced polymer composites, have proved to be a suitable alternative. One of the important tests that conventional and composite materials have to undergo is fatigue test. It refers to the testing of materials for their cyclic behavior. In fatigue testing, depending on the choice of the researchers, materials are loaded till reaching their failure or till reaching a fraction of the total stiffness loss. Composite materials are different from metals and they show a distinct behavior under fatigue loading. In metals, failure occurs from the commencement of a single crack and then its propagation. In composite materials, conversely, it is a complex process as these materials possess crack-arresting properties. This review paper highlights various aspects of the cyclic or fatigue behavior in composite materials. Factors triggering such behavior in composite materials include reinforcing substance, matrix material, fiber orientation or stacking sequence, fiber content, testing environment and so on, together with the damage development process at the microscopic level. Loading condition parameters pertain to stress ratio, mean stress, loading condition, multiaxial stress, and testing frequency. This article also includes the effect of carbon nanotubes on the fatigue life of the polymer composites. POLYM. COMPOS., 00:000–000, 2016. © 2016 Society of Plastics Engineers

INTRODUCTION

Carbon fibers and glass fibers are the two major reinforcing materials for polymer composites. Polymer-based matrix together with the above two reinforcements offer a vast range of materials that are light weight, possess superior mechanical properties and have better resistance against adverse environment and corrosion. These materials are now replacing conventional materials in the field of aeronautics [1], automation [2], marine vessels [3], wind turbine blades [4], underground oil drilling [5], and so forth. In all these fields of industrial activities, the composite undergo cyclic or fatigue loading. Most of the composite products are in laminated forms (other than whiskers and particulate). Moreover, ply orientation together with their thickness play a vital role in deciding the properties of the products [6]. As far as application in the referred fields are concerned, mechanical properties of the composite are seriously damaged by delamination, fiber breakage and/or matrix crushing in fatigue loading.

Hand layup, resin transfer moulding (RTM), vacuum assisted resin transfer moulding (VARTM) [6], are some of the common methods to make laminated products from fiber fabrics. The commonly used fiber fraction is 30–60% and it primarily depends on the type of the composite that is going to be used. Commonly used materials in fiber form for the reinforcement are glass, carbon, and boron as well. Among these reinforcing resources, glass is the most common fiber that is used and it comprises more than 90% of the manufacturing exercises [7]. Glass fibers are of three types, that is, E-glass, S-glass, and C-glass. Of them, S-glass is the strongest and E-glass is the most used one. The amount of silica oxide (SiO_2) together with oxides of boron, calcium, aluminum, iron, and sodium are used in different proportions in the referred types of glasses. As a result, they possess different physical properties [8]. Table 1 [8] shows chemical composition and physical properties of three different types of glass fibers. Other than glass fibers, carbon fibers have also been studied in the present exercise. In general, 90% of the carbon fibers are made of polyacrylonitrile [8] and the rest is made of petroleum pitch and rayon. These fibers possess excellent modulus, strength, dimensional accuracy at higher temperature, high thermal conductivity, and low coefficient of thermal expansion as compared to the glass fibers. However, compared to glass fibers, carbon fibers possess low impact strength.

In 1991, Sumio Iijima [9] discovered needle-like structure of carbon, now known as "Carbon nanotubes" (CNTs) [9]. The excellent mechanical properties of the CNTs, such as, elastic modulus which can go upto 1TPa [10], tensile strength upto 200GPa [11] and elongation to failure upto 15% [12] make CNTs the most promising material for modification of the matrix in fiber reinforced

Correspondence to: A. Gaurav; e-mail: anandgaurav1303@gmail.com
DOI 10.1002/pc.24177
Published online in Wiley Online Library (wileyonlinelibrary.com).

TABLE 1. Glass fiber composition and properties.

	E-glass	C-glass	S-glass
Composition (%)			
SiO_2	52.4	64.4	64.4
$Al_2O_3 + Fe_2O_3$	14.4	4.1	25.0
CaO	17.2	13.4	–
MgO	4.6	3.3	10.3
$Na_2O + K_2O$	0.8	9.6	0.3
B_2O_3	10.6	4.7	–
BaO	–	0.9	–
Properties			
ρ (Mg m^{-3})	2.6	2.49	2.48
K (W m^{-1} K^{-1})	13	13	13
α (10^{-6} K^{-1})	4.9	7.2	5.6
σ_u (GPa)	3.45	3.30	4.60
E (GPa)	76.0	69.0	85.5
T_{max} (°C)	550	600	650

polymer composites. In this context, Zou et al. [13] reported 45% improvement in tensile strength and 90% in the modulus of epoxies with CNTs as compared to epoxies without them. This review paper highlights the fatigue life and fatigue behavior of the carbon fiber and glass fiber reinforced polymer composites with and without CNTs. The study has been primarily based on the literature of the previous 20 years. Moreover, where necessary, older papers were reviewed for essential information.

Thermosets and thermoplastics are two major categories of polymer matrix. Polymer matrix is the gathering of a large number of polymer molecules of like chemical structure. Epoxies, polyesters, polyimides are a few of the commonly used thermosets, each having its own field of application. Nylons, polycarbonates, and polyamide-imide, conversely, come under thermoplastics. Thermosets do not get affected by heat. They rather burn but do not change their shape when exposed to heat. Therefore, thermal stability, creep resistance, high impact strength, and fracture resistance are a few of the important properties of thermosets. However, when compared to thermoplastics, long curing duration and low strain prove to be their major shortcomings. Thermoplastics, conversely, fail at higher strain in comparison to thermosets. Major advantages of the thermoplastics are unlimited shelf life, low curing duration, and the ability to reform and reshape by application of heat [6]. Figure 1 makes a comparison of tensile stress and strain in Epoxy (thermoset) and polysulfone (thermoplastic).

FATIGUE OF POLYMER COMPOSITES

Composite materials are heterogeneous and anisotropic. Thus, unlike metals, damage spreads to the entire area of composite materials rather than in a localized manner as happens in metals. For metals, damage is initiated by propagation of a single crack but in composite materials fiber breakage, matrix cracking, delamination, matrix-fiber debonding, transverse-ply cracking, or combination of any of them can trigger damage [14]. These failure parameters are highly influenced by material properties and testing conditions. Other than these, discontinuities in the geometrical appearances, as evident in holes, sharp corners and change in the thickness of the sample, causes stress concentration. Reifsnider et al. [15] considered the following three points for analysis of damage development in composite materials under quasi-static and cyclic loading;

1. Exact, accurate and detailed nature of damage development in the laminated composites together with damage mechanism and duration of damage process.
2. Description of the "damage state" resulting in a loss of strength and stiffness. It is impractical to analyze a failure from an undamaged state.
3. Use of experiment data to develop a damage model, which can help to optimize utilization of the material.

Polymer matrix composites fail under low strain. Thus, making it a difficult task to conduct low cycle fatigue test on it. In this regard, Agarwal et al. [16] conducted a low cycle as well as high cycle fatigue test on glass fiber reinforced polymer under frequencies of 0.01 and 2 Hz. The tests were strain-controlled with a stress ratio (R) of 0.05. The strains were monitored by 2 inch-extensometers. As many as 45 specimens were tested in low cycle range and 20 samples were tested in high cycle range, making it a total of 65 specimens. The S–N curve was defined within a range of 3 to 10^6 cycles. Figure 2 shows S–N curve of the GFRP composite.

Fatigue of Woven Fabric

A laminated composite can be categorized on the basis of the direction of its fibers. It can be of unidirectional lamina or in the form of 3D woven textile. In general, unidirectional lamina is available in prepreg or pre-impregnated form. Woven textiles are present in the form of 3D weave, advanced braiding and knitted. These textiles are used to prepare laminate by hand moulding, RTM or VARTM. These fabrics offer an additional

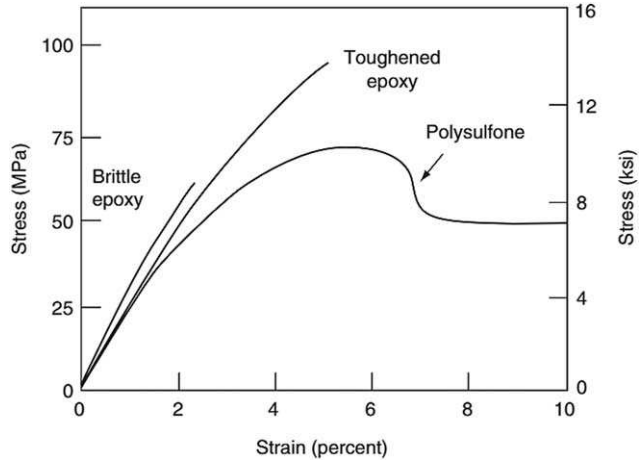

FIG. 1. Tensile stress strain diagram of a Thermoset (epoxy) and Thermoplastic (PS) [6].

 DOI 10.1002/pc

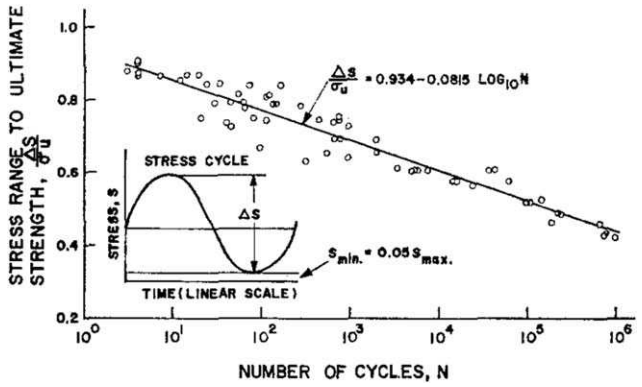

FIG. 2. Fatigue strength of GFRP under strain controlled test ($R = 0.05$) [16].

benefit of reinforcement along the thickness of the laminate. As a result, there is an increase in stiffness and in-depth strength, enabling the manufacturer to tailor the properties in any direction according to the load application. A general presentation of plain woven fabric lamina has been made in Fig. 3. Assuming warp to be in loading direction and fill to be in orthogonal direction, damage can be noticed to have accumulated or failure occurred in warp, fill or resin-rich region (pure matrix region) [14].

MATERIALS AND TESTING

Brunbauer et al. [17] conducted a comparative experiment on carbon fiber reinforced epoxy laminate with 30% and 55% of fiber fraction (v_f), prepared by VARTM. The ply orientations were 0°, 45°, and 90°. Tension–tension fatigue (TTF) tests were carried out with $R = 0.1$ and tension–compression fatigue tests were carried out with $R = -1$. The test frequencies were in the range of 2–10 Hz. For each stress level, the minimum number of specimens tested was three so as to generate the S—N curve. The curve showed that the graph is steeper in case of tension–compression fatigue compared to TTF tests.

Zhang et al. [18] worked on the fatigue life prediction model of GFRP composites. The residual stiffness model and the strain failure criterion were used to establish that fatigue failure in GFRP is brittle in nature. The testing was carried out according to the ASTM 3039 standard for both on-axis and off-axis loadings. Sinusoidal wave form was used with R varying from 0.1 to 10. Experiments were carried out at room temperature. Fiber volume fraction was in the range of 0.36 to 0.67. Stiffness degradation model was proposed by the equation

$$\frac{dE(n)}{dn} = -E(0)Qvn^{v-1} \quad (1)$$

where E (0) is the initial stiffness, n is the number of loading cycles, and Q and v are the parameters depending on applied stress, frequency, and stress ratio. The above equation is based on the assumption that residual modulus is a monotonically decreasing function of a number of cycles (n). Fiber volume fraction was not considered as one of the variables. However, as initial stiffness is calculated as the weighted mean of fibers and matrix moduli in fiber-based composites, any increase in the fiber volume will increase stiffness of the laminate upto a practical limit of 55–60% in unidirectional fiber laminate [19].

Knoll et al. [20] studied the effect of carbon nanoparticles on the fatigue performance of carbon fiber reinforced epoxy. Böger et al. [21], conversely, made a comparative study of the fatigue life of glass fiber reinforced epoxy, enhanced with 0.3 wt% of fumed silica SiO_2 and multi-walled carbon nanotubes (MWCNTs). The stress ratios were $R = 0.1$ for TTF, $R = -1$ for tension–compression and $R = 10$ for compression–compression fatigue test. Test frequency was set at 6 Hz to avoid self-heating of the specimen. Reduction in the maximum stress amplitude increased the fatigue life of both modified and unmodified matrix composites. Presence of MWCNTs increased the static strength of the composite, thus increasing the maximum stress amplitude of the material. The slope of the lines for both the composites were observed to be the same in TTF test (Fig. 4a) although life of the material was prolonged by one order of magnitude in load cycles. In tension–compression fatigue test, addition of MWCNTs to the matrix showed even better results. Slope of the S-N line in the modified matrix composite was less when compared with an unmodified matrix. Although, at higher stress levels, life of the composites was almost equal, down the line, life was prolonged by orders of magnitude. Compression–compression fatigue test also showed improved fatigue life of MWCNT modified matrix composites (Fig. 4b). This improvement was even greater when compared to the tension–compression test due to the presence of a pure compression region. In compression–compression test, fiber buckling is a limiting factor, which is overcome by stiffer modified matrix. Knoll et al. [20] showed that the fatigue life of CFRP could be increased by adding 0.3% of MWCNTs in the matrix material. Moreover, if the CNTs added were of few layers or close to the single

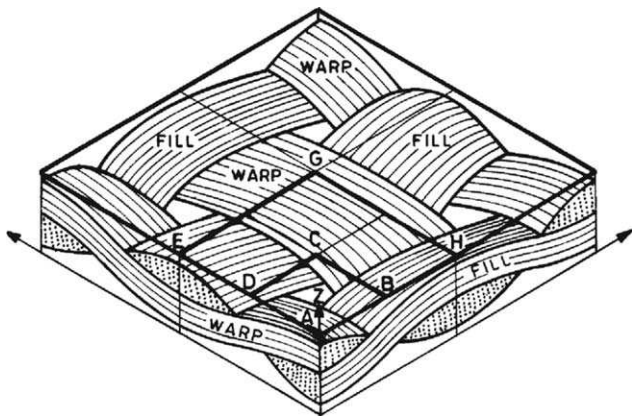

FIG. 3. Ideal plain weave lamina [14].

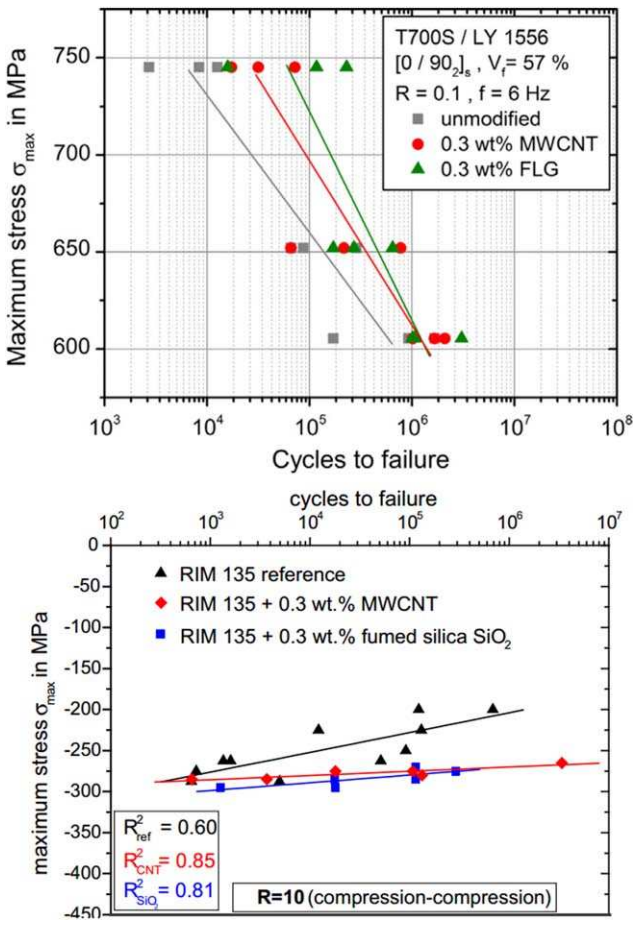

FIG. 4. Increase in fatigue life by adding 0.3 wt% of CNTs in (a) tension–tension fatigue test [20]; (b) compression–compression fatigue test [21]. [Color figure can be viewed in the online issue, which is available at wileyonlinelibrary.com.]

walled carbon nano tube, the fatigue result could be further improved.

Wu et al. [22] studied the fatigue behavior of FRP and hybrid FRP sheets. Their study included laminates, made up of glass, carbon, polyparaphenylenl benzobisoxazole (PBO), and basalt fibers with epoxy matrix. Hybrid composite sheets were made using different layers of two different materials. For instance, carbon/glass and carbon/basalt FRP layers were used in the ratio of 1:1, that is, for each layer of carbon, one layer of glass or basalt was used with nominal fiber volume fraction of 50%. TTF tests were conducted with stress ratio (R) of 0.1 and loading frequency of 5 Hz. According to the experiments, CFRP and PBOFRP composites showed better resistance toward cyclic loading when compared to the GFRP and BFRP composite laminates. A total of 12 specimens of CFRP, PBOFRP and BFRP laminates were tested, whereas the number of specimens, made of GFRP and carbon/glass hybrid laminates, tested was 10. Moreover, nine specimens of carbon/basalt hybrid laminate were considered. In static testing, the PBOFRP composite showed the highest tensile modulus of 266 GPa, followed by CFRP (242 GPa) and Carbon-Basalt FRP (166 GPa). Conversely, the GFRP composite showed the least tensile modulus of 87 GPa preceded by BFRP (91 GPa) and carbon-glass hybrid FRP (162 GPa). In the TTF test, for which two million cycles were considered as runout cycles, the CFRP and PBOFRP laminates showed the highest fatigue limit of 83.7 and 76.7% of the ultimate strength. Again for the GFRP and BFRP composites, the same limit was at 61.3 and 55%. In hybrid composite, C-BFRP laminate had a higher limit of 70% when compared to C-GFRP hybrid laminate, which had a fatigue limit of only 58% of the ultimate strength.

A number of researchers have contributed with different materials and testing parameters. Table 2 presents a consolidated view of the materials and parameters used by different scholars in their work.

DAMAGE MECHANISM

Damage mechanism in a polymer matrix reinforced with fiber is a complex process to explain. Reifsnider et al. [56] recognized three phases of fatigue life. Each phase varies with the other in failure mode. Micromechanics together with meso-model [57] for the laminates can be a useful tool for assessment of damage mechanism. To find the most efficient damage theory for the FRP composites, World Wide Failure Exercise [58] was initiated. Major damage mechanisms, which can be observed in the fatigue of fiber-based composites, are fiber breakage, matrix cracking, fiber/matrix debonding, delamination and fracture as a whole component. According to Vasiukov et al. [59], damage mechanism can considered to be a non-linear function of a number of cycles. If samples are free of stress concentrations [26, 31], then damage growth is fast at the beginning and at the end of the cyclic loading. However, in the middle of the phase, damage propagation is linear in nature [14]. The magnitude of damage depends on property of each lamina, stacking sequence, and interface property of the laminate. In general, there are three stages of failure. Stage 1 starts with debonding of the matrix/fiber interface at the beginning of micro-cracking of the matrix material. Figure 5a shows saturation of the crack in cyclic loading whereas in Fig. 5b black lines show damage buildup within the cycles of the unmodified matrix. Stage I, which shows damage initiation, is steep when plotted against fatigue cycles and so is stage III, which is the end of the cycle. Stage II is almost linear in nature. Addition of CNTs has remarkable effect on three phases or stages of the damage accumulation. Figure 5b shows the effect of adding nanoparticles. From this figure, one can conclude that addition of nanoparticles (modified matrix) shifts the damage buildup downwards as compared to the unmodified matrix. Also, fatigue life of the modified matrix increases considerably.

DOI 10.1002/pc

TABLE 2. Materials and parameters.

Sl. No.	Year	Author	Matrix	Fiber	Fiber vol%	*R*	Hz	t–t	t–c	c–c	Nanoparticles
1	2014	Borrego et al. [23]	Epoxy	Glass	–			√			0.5% MWCNT
2	2013	Takeda et al. [24]	Bisphenol-F Epoxy	Glass	56	0.1	4	√			0.5% MWCNT
3	2013	Kennedy et al. [25]	Epoxy	Glass	50	0.1	3 and 6	√			
4	2013	Nixon-Pearson et al. [26]	Epoxy	Carbon		0.1	5	√			
5	2013	Gude et al. [27]	Epoxy	Carbon	60	−1	180		√		0.3% CNT
6	2012	Esmaeillou et al. [28]	Polyamide 66	Glass	30	0.1 or 0.3	2 to 60	√			
7	2011	Vavouliotis et al. [29]	Epoxy	Carbon	58	0.1	5	√			0.5%MWCNT
8	2011	Baere et al. [30]	PPS	Carbon			5 and 2	√			
9	2011	Bizeul et al. [31]	Epoxy	Glass	50		20				
10	2011	Hosoi et al. [32]	Epoxy	Carbon	57	0.1	100	√			
11	2010	Bizeul et al. [33]	Epoxy	Glass	50		20				
12	2009	Goel et al. [34]	Polypropylene	Glass	21		10 to 20				
13	2009	Hosoi et al. [35]	Epoxy	Carbon	60	0.1	5 and 100	√			
14	2008	Botelho et al. [36]	Epoxy	Carbon	60	0.1	8	√			
15	2008	Grimmer et al. [37]	Epoxy	Glass	56	0.15	3	√			1% CNT
16	2007	Cavatorta [38]	Epoxy	C, G	55						
17	2007	Kawai et al. [39]	Epoxy	Carbon		(.1,.5), (−1, 0.68), (10,2)		√	√	√	
18	2006	Shindo et al. [40]	Epoxy	Glass	47	0.1	4 and 10	√			
19	2005	Kumagai et al. [41]	Epoxy	Glass	47	0.1	1, 4,16	√			
20	2004	Bureau et al. [42]	Polypropylene	Glass	60	0.1	5				
22	2004	Pandita et al. [43]	Epoxy	Glass		0.1	0.5 to 10	√			
23	2003	Gassan et al. [44]	Epoxy	Glass		0.1	5 and 10	√			
24	2002	Vina et al. [45]		G, C	30, 35		3				
25	2002	Yokozeki et al. [46]	Epoxy	Carbon		0.1	5	√			
26	2002	Tong [47]	Epoxy	Glass	62	0.1	10	√			
27	2001	Barron et al. [48]	Epoxy	Carbon		0.1	5, 10, 20	√			
28	2001	Pandita et al. [49]	Epoxy	Glass	50	0.1	0.5 to 10	√			
29	1999	Ogihara et al. [50]	Epoxy	Carbon	55	≈0	5	√			Polyamide
30	1999	Takeda et al. [51]	Epoxy	Carbon	55, 64	0	5	√			
31	1998	Whitworth [52]	Epoxy	Graphite		0.1	10	√			
32	1998	Demers [53]	Vinyl-ester	Glass	38	0.05, 0.1, 0.5	1, 3, 5	√			
33	1997	Wang et al. [54]	Epoxy	Carbon	52	0.05	0.5	√			
34	1995	Ma et al. [55]	PEEK	Carbon	60	0.1	10	√			

c = carbon, **g** = glass, **t–t**= tension–tension fatigue test, **t–c**= tension–compression fatigue test, **c–c**= compression–compression fatigue test, ***R*=** stress ratio, **Hz=** test frequency, **CNT**= carbon nano tubes, **MWCNT**= Multi walled carbon nano tubes.

FIBER VOLUME FRACTION

A basic mean to describe a composite laminate is its fiber volume fraction. Fiber volume fraction is defined as the ratio of the amount of fibers to the matrix as present in the laminate. The higher the fiber volume, the higher will be the load carrying capacity of the laminate. However, there is an upper limit to this. As the fiber content increases, the amount of matrix decreases. When load is applied, the matrix holds fibers in their respective places. Therefore, the matrix plays a vital role in load carrying capacity as well. If the matrix amount gets reduced, strength of the composite gets compromised. The optimum value for the fiber volume fraction is 45–60%. In this respect, based on fiber volume fraction, a number of researchers have established results as far as the fatigue behavior of the laminate is concerned.

Brunbauer et al. [17] carried out a comparative study on carbon/epoxy system with 30 and 55% of fiber volume fraction together with different fiber orientations, that is, 0°, 45°, and 90°. In TTF test, enhancement of fiber volume fraction from 30 to 55% led to an increase in the nominal stress of 40% in 90° unidirectional laminate. This effect was backed by a theory explaining that in low fiber fraction, the dominant damage mode is matrix cracking and fiber matrix debonding. Conversely, in high fiber fraction, the damage mode was fiber pullout. However, in tension–compression test, there was not much variation in the results for both the samples with 30 and 55% fiber volume. With unidirectional laminate at 45° fiber orientation, higher fiber volume fraction resulted in higher fatigue strength. With unidirectional laminate at 0°, tension–tension loading led to fiber pullout fracture or single fiber breakage. Conversely, in tension–compression loading, fiber bundle breakage along the fractured plane was observed. Stress–strain hysteresis showed that in tension–tension testing, the hysteresis shifted toward the higher strain zone whereas in tension–compression loading, the stress–strain hysteresis was reversed, which indicated decrement in tensile and compression stiffness. This could be due to unremitting rise in fiber breakage because of compressive loads that weaken the tensile and

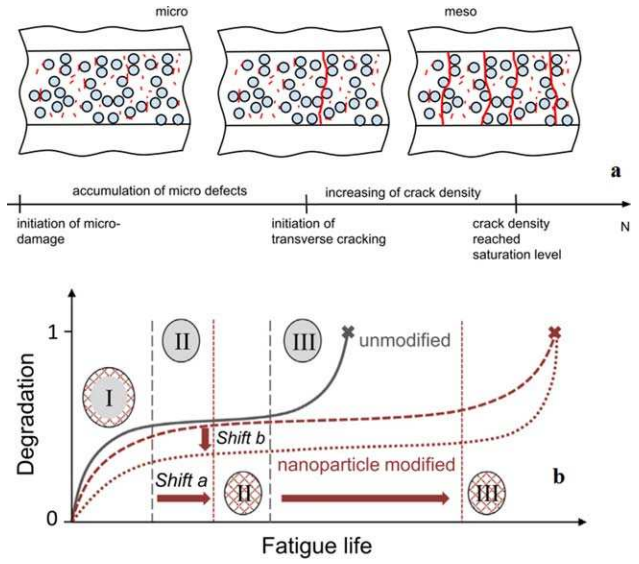

FIG. 5. (a) Saturation of cracks in cyclic loading [59]; (b) adding CNTs enhance fatigue life of composite [20]. Black line shows degradation rate of unmodified matrix, while dotted red line show degradation rate of matrix modified with CNTs. [Color figure can be viewed in the online issue, which is available at wileyonlinelibrary.com.]

compressive behavior of the sample. Figure 6 compares the fatigue life of FRP with different fiber fractions. A summary of the experiment can be seen in Fig. 7, which shows mechanical behavior and damage mechanisms in carbon/epoxy laminate, depending on the fiber direction, fiber fraction and loading type, respectively.

Mini et al. [60] studied the fatigue behavior of glass/epoxy composite materials with fiber volume fraction of 34.4, 38.93, 48.88, and 57.01%. The mean stress was zero, indicating that the tests were completely reversible in nature, that is, $R=-1$. The loading frequency was 7.33, 8.17, and 9 Hz, respectively. Composites of different fiber volume fractions were tested at each frequency. It was concluded that in a composite, with lower fiber volume fraction, stiffness reduction is gradual with an

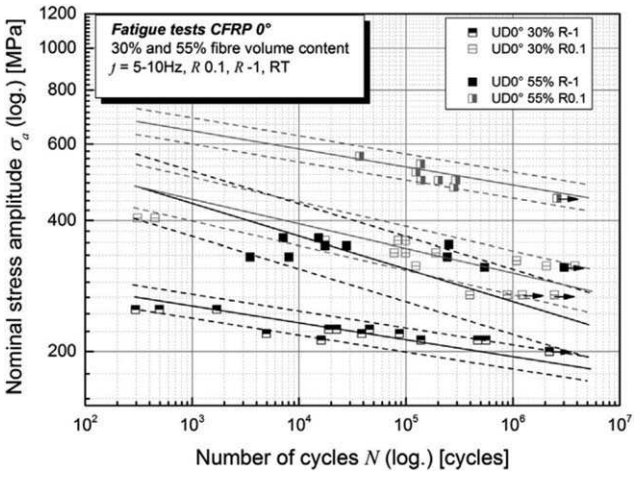

FIG. 6. Comparison of fatigue life laminates with two different fiber volume fraction, that is, 30 and 55% [17].

increase in cycles due to matrix cracking. It then reaches a constant value. Conversely, in a composite with higher volume fraction, the loss of stiffness is sudden. This is due to fiber cracking as a smaller amount of matrix is present to avoid shearing of the fibers.

MEAN STRESS AND STRESS RATIO

Maximum stress (σ_{max}) and minimum stress (σ_{min}) are the two components of cyclic loading. Mean stress is the average of these two types of stresses, induced in the component. This is expressed by Equation *2* and the stress ratio, which is the ratio of the minimum stress (σ_{min}) to the maximum stress (σ_{max}), is expressed by Equation *3*. In other words, we can say that mean stress defines stress ratio and vice versa.

$$\sigma_{mean}=\frac{\sigma_{max}+\sigma_{min}}{2} \tag{2}$$

$$R=\frac{\sigma_{min}}{\sigma_{max}} \tag{3}$$

Stress ratio (R) formulates fatigue loading with $1<R<+\infty$ indicating that the cycle is in compression–compression region, $-\infty<R<0$ indicates that the cycle is in tension–compression region and $0\leq R<1$ indicates that the cycle is in tension–tension region. A more comprehensive picture is presented in Fig. 8 [14], where,

1 = Compression–compression region	7 = Fully reversed cycle
2 = Tension–compression region	8 = Tension dominated alternating cycle
3 = Tension–tension region	9 = Alternating cycles
4 = Compression–compression cycle	10 = Zero tension cycle
5 = Zero compression cycle	11 = Tension–tension cycle
6 = Compression dominated alternating cycle	12 = Time

Schütz et al. [61] conducted a series of experiments on carbon/epoxy unnotched laminate with different stress ratios, that is, 0.1, −0.5, −1.0, −1.66, and −5.0. A more complete picture of the fatigue behavior for various mean stresses emerges by presenting the tests in a constant life diagram. Constant life line for 50% probability of survival for mean stress has been plotted against loading stress. The ultimate strength of the specimen in tension and compression is equal. Figure 9 shows the relation between stress amplitude and mean stress (constant fatigue life [CFL] diagram). From the figure, one can conclude that mean stress has a significant effect on fatigue life.

Kawai et al. [39] conducted fatigue tests on carbon/epoxy system with two different quasi-isotropic laminates ($[45/90/-45/0]_{2s}$ and $[0/60/-60]_{2s}$) and one cross-ply laminate ($[0/90]_{3s}$) at six different stress ratios of 0.5, 0.1,χ, −1.0, 2 and10, where χ is the critical stress ratio and is given by $\chi=\frac{\sigma_C}{\sigma_T}$ with σ_C being the ultimate compressive strength and σ_T being the ultimate tensile

DOI 10.1002/pc

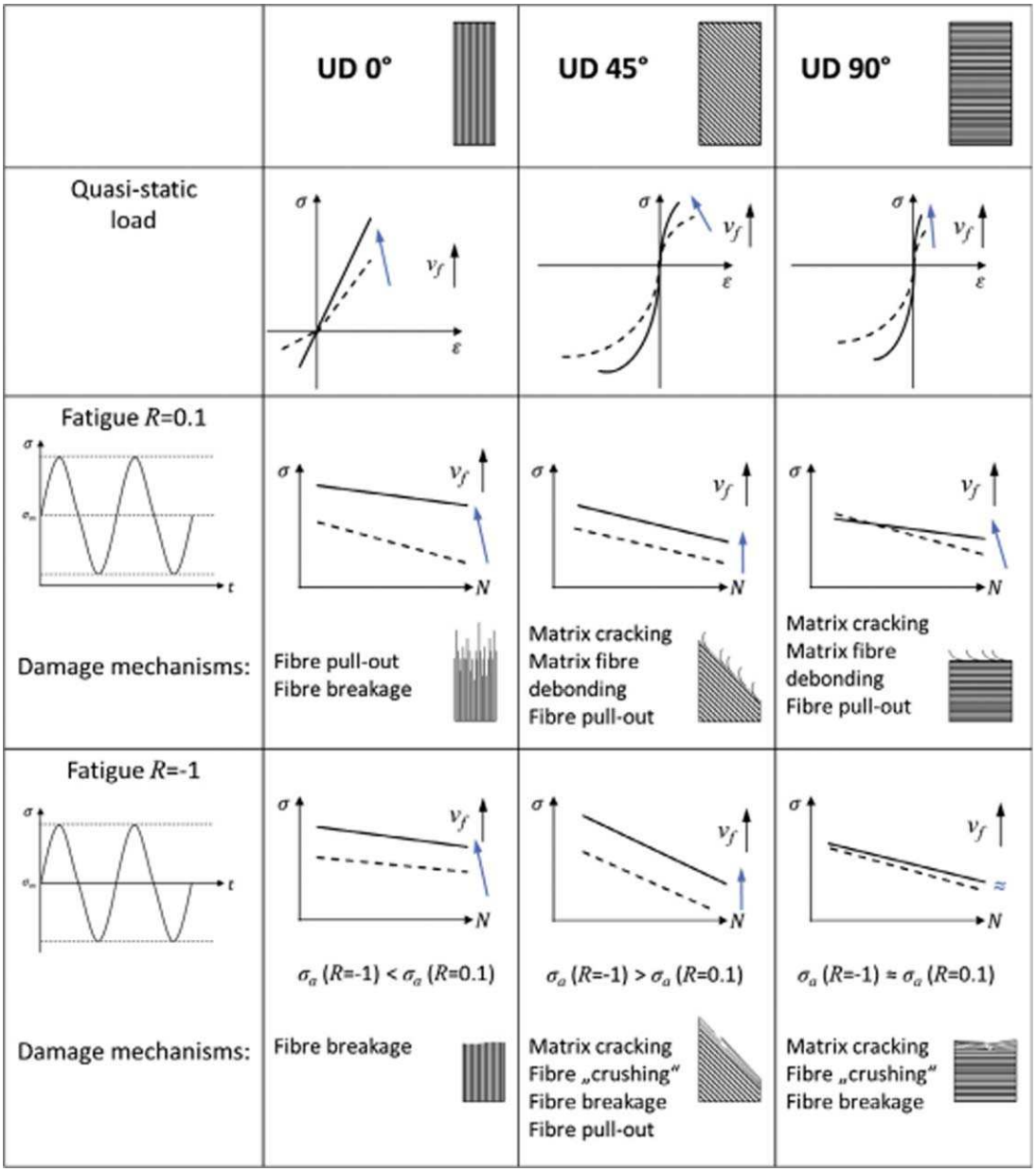

FIG. 7. Mechanical behavior and damage mechanism in carbon/epoxy laminate with different fiber direction, fiber volume fraction, test angle, applied load type, and fatigue mean stress [17]. [Color figure can be viewed in the online issue, which is available at wileyonlinelibrary.com.]

strength of the specimen, respectively. A total of 14 samples were earmarked for static tests from which three samples were tested for the ultimate strength in tension and three for the ultimate strength in compression for quasi-isotropic laminates. For cross-ply laminates, one sample each was used for the same tests. Later, critical stress ratio was calculated to be −0.68, −0.53, and −0.44 for the three respective layups, explained earlier. It was found that the quasi-isotropic laminate with $[0/60/-60]_{2s}$ layups had very low compressive strength. This was attributed to the fact that in absence of its cross ply, outer fibers at 0° fails as a result of out-of-plane micro-buckling. Hence, the [0/60/−60] layup fails as well by out-of-plane micro-buckling, which caused it to possess low compressive strength. S–N plot of the $[45/90/-45/0]_{2s}$ layup showed that slope of the life at $R = \chi = -0.68$ is steeper than that of at $R = 0.1$ and −1. In the T–C testing, the composite was found to be more responsive toward cyclic loading than in the T–T testing, which becomes even more sensitive when the stress ratio gets closer to the critical stress ratio.

The graph of CFL (Fig. 10a) was plotted for quasi-isotropic laminate with ply orientation of $[45/90/-45/0]_{2s}$. As far as the short fatigue life is concerned, the CFL diagram was found to be almost linear in nature and it became nonlinear with an increased fatigue life.

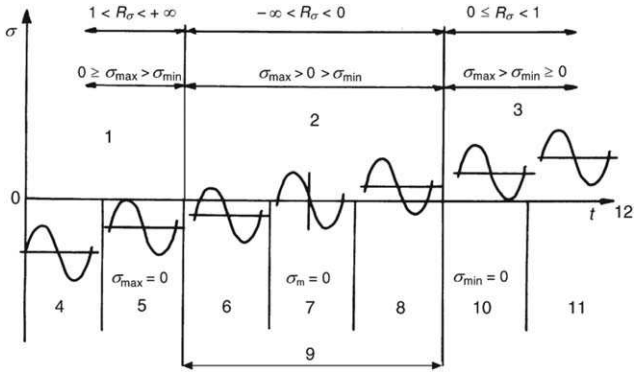

FIG. 8. Fatigue cycle classification [14].

The following assumptions were made in this experiment for drawing an efficient CFL diagram or asymmetric anisomorphic CFL diagram.

1. For a given value of stress life N_f, the amplitude σ_a of the alternating stress becomes the maximum at a critical stress ratio χ.
2. With an increase in the fatigue life, the CFL curve changes its shape from a straight line to a parabola.
3. Two straight lines connecting the peak point (σ_m^{peak}, σ_a^{peak}) bounds the static failure region in a CFL diagram, with σ_T and σ_c being the tensile and compressive strength of the specimen.

The theoretical CFL curve can be explained as a function of different formulae, which depends on the position of the mean stress σ_m in the domain $[\sigma_c, \sigma_T]$ as follows:

$$-\frac{\sigma_a-\sigma_a^{\chi}}{\sigma_a^{\chi}}=\begin{cases}\left(\dfrac{\sigma_m-\sigma_m^{\chi}}{\sigma_T-\sigma_T^{\chi}}\right)^{(2-\psi_{\chi})}; & \sigma_T \geq \sigma_m \geq \sigma_m^{\chi}\\ \left(\dfrac{\sigma_m-\sigma_m^{\chi}}{\sigma_c-\sigma_m^{\chi}}\right)^{2-\psi_{\chi}}; & \sigma_C \leq \sigma_m < \sigma_m^{\chi}\end{cases} \quad (4)$$

where σ_a^{χ} and σ_m^{χ} are the alternating and the mean stress at the critical stress ratio and ψ_{χ} is the fatigue strength ratio at the critical stress ratio, which is given by

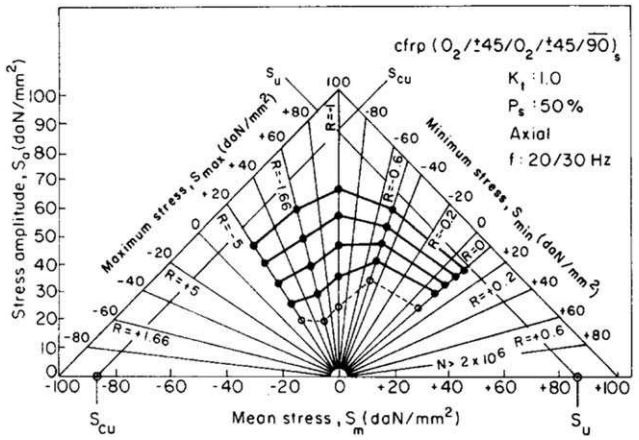

FIG. 9. CFL diagram of carbon epoxy unnotched sample [61].

$$\psi_{\chi}=\frac{\sigma_{\max}^{\chi}}{\sigma_B} \quad (5)$$

where $\sigma_B(>0)$ is the reference strength. The anisomorphic CFL diagram is shown in Fig. 10b. For anisomorphic CFL diagram, parabolic curve was obtained.

LOADING FREQUENCY AND HYSTERESIS HEATING

Loading frequency or testing frequency has a significant effect on the fatigue life of fiber reinforced polymer composites. Loading frequency is also known as the strain rate. Attempts have been made to study the effects of frequency on fatigue testing of polymer composites. One of the major effects of loading frequency is self-heating or hysteresis heating of the sample. Since polymers are visco-elastic in nature, testing at high frequency leads the matrix toward the glass transition temperature (T_g). At this temperature, the polymer starts to convert into soft rubbery material from glassy brittle material, changing properties of the polymer composite in the process.

Gude et al. [27] tested carbon/epoxy composite at a very high frequency of 180Hz with a newly developed machine. This device can conduct shaker-based fatigue tests with very high frequency ($f > 150$ Hz) without much heating of the specimen. During the tests samples were loaded without pre-stress ($R = -1$), with fiber strain $\varepsilon = 0.02$ and frequency of 180 Hz. Despite conducting the fatigue test only on a carbon/epoxy system, no findings could be gathered regarding the modified matrix with 0.3 wt% of CNTs. The use of 3-ball-mill was emphasized to

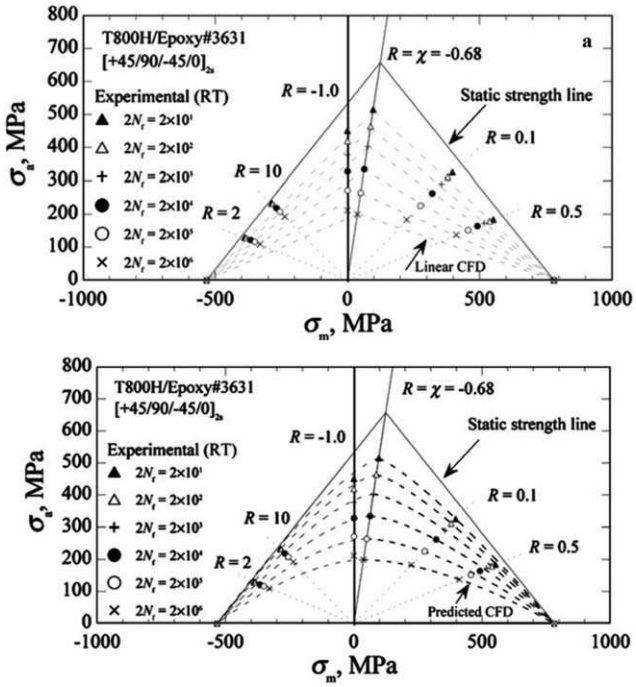

FIG. 10. (a) Constant fatigue life (CFL) graph [39]. (b): Anisomorphic CFL diagram [39].

DOI 10.1002/pc

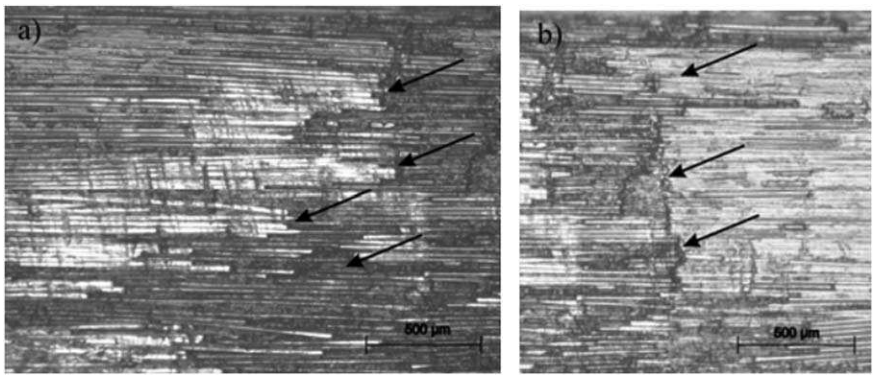

FIG. 11. Micrographs of damaged fibers [27].

get superior dispersion of CNTs in the epoxy. The damage in the unmodified matrix composite was observed after 9.7×10^7 cycles. Figure 11 shows micrographs of the damaged fibers during handling which resulted in a significant drop in stiffness during the tests.

Esmaeillou et al. [28] conducted fatigue experiments on glass/polyamide 66 at different frequencies of 2, 10, and 20 Hz and various applied loads. The experiments were conducted with alternate flexural fatigue (AFF) test with $R = -1$ and TTF test with $R = 0.3$. TTF at 10 and 20 Hz showed the same properties upto 10^4 cycles, which was noted as zone I. The zone II, which came after 10^4 cycles, showed significant deviation in the properties. When it came to the AFF test, the S–N curve for 2 and 10 Hz tests were superimposed upto 10^3 cycles. However, the same test at 20 Hz showed deviation from the starting point of the experiment. For the same applied stress, if the frequency is higher, then the material fails earlier. Hence, one can conclude that increased frequency lowers the life of a sample. One more significant effect of the loading frequency was increase in temperature. It hampers the material properties, or, in other words, the stress induced in the specimen decreases as shown in Fig. 12a. The TTF tests were conducted at 10 and 20 Hz at a nominal stress of 66 MPa. From Fig. 12b [28], it is clear that frequency has a direct effect on the temperature and on the material failure. AFF tests at $\varepsilon = 0.019$ and frequency of 2, 10, and 20 Hz showed that an increased frequency lowered the material strength and increased the temperature of the specimen.

Goel et al. [34] studied the effect of stress amplitude on the temperature of PP and LFT samples at frequencies of 10, 15, and 20 Hz, respectively. In terms of loading frequency and fatigue life, the results were in accordance with the literature that established that an increase in frequency decreases fatigue life. As polymers have poor thermal conductivity, it is obvious that there would be a considerable rise in the temperature. It was also observed that the temperature rise/hysteresis loss in un-reinforced PP is much higher than LFT. In PP samples, mobility and sliding of polymer chains caused high degree of hysteresis loss. This movement was hindered by fibers upto a certain extent in LFT, resulting in less hysteresis loss. Figure 13 shows temperature rise as a function of stress amplitudes of 21, 27, and 35 MPa at 10 Hz frequency.

Pandita et al. [43] explored the fatigue performance of epoxy, reinforced with various types of knitted glass fiber loaded in the weft and bias direction. The TTF test of warp knitted, weft knitted and plain weave fabric reinforced epoxy was carried out at frequencies ranging from 0.5 to 10 Hz and $R = 0.1$. According to the investigation, fatigue performance of woven fabrics was higher than the knitted fabrics. The lower fatigue performance of the knitted fabrics was due to a lower fiber fraction and lower ultimate strength of the material. In bias direction, the fatigue performance of the material was highly influenced by the fiber matrix interaction. Hysteresis heating of the

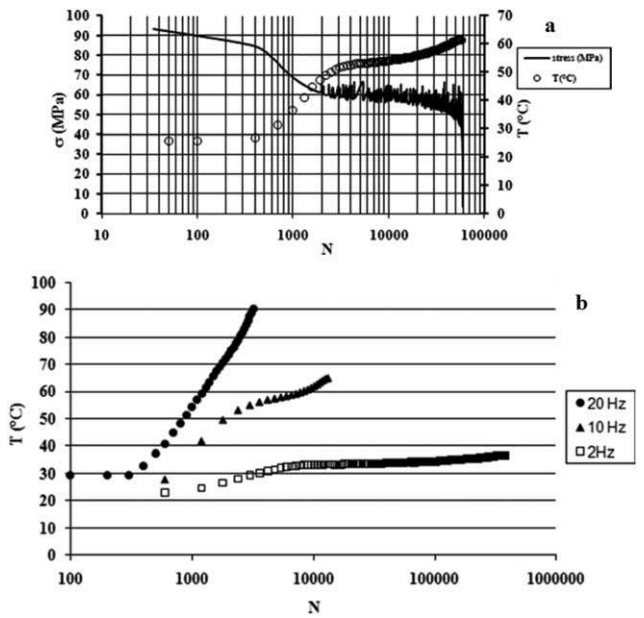

FIG. 12. (a) Increasing temperature hampers mechanical properties [28]; (b): Frequency has a direct effect on the temperature and so on the material failure [28].

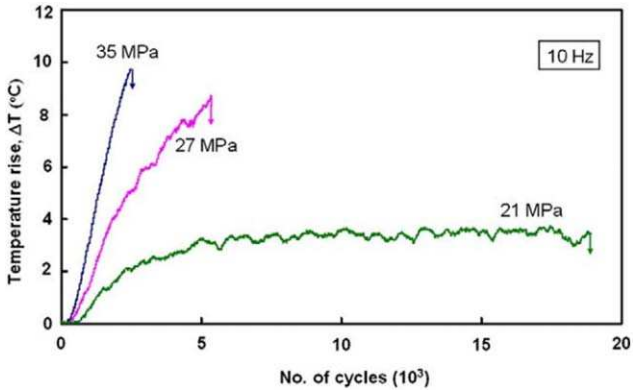

FIG. 13. Effect of stress on fatigue life [34]. [Color figure can be viewed in the online issue, which is available at wileyonlinelibrary.com.]

knitted and woven fabric composites was studied at 3 and 5 Hz. At a frequency of 5 Hz, the temperature of the woven fabric laminate reached the glass transition temperature promptly which did not happen for the knitted fabric. At a frequency of 3 Hz, the hysteresis heating was

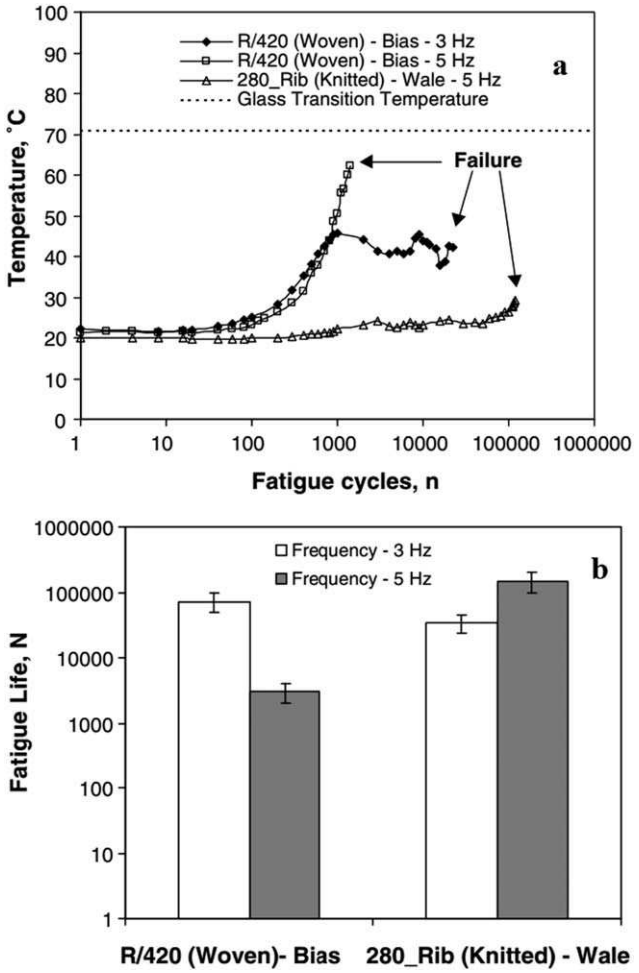

FIG. 14. (a) Effect of fiber weaving on hysteresis heating [43]. (b): Increase in fatigue life by matrix toughening due to temperature rise [43].

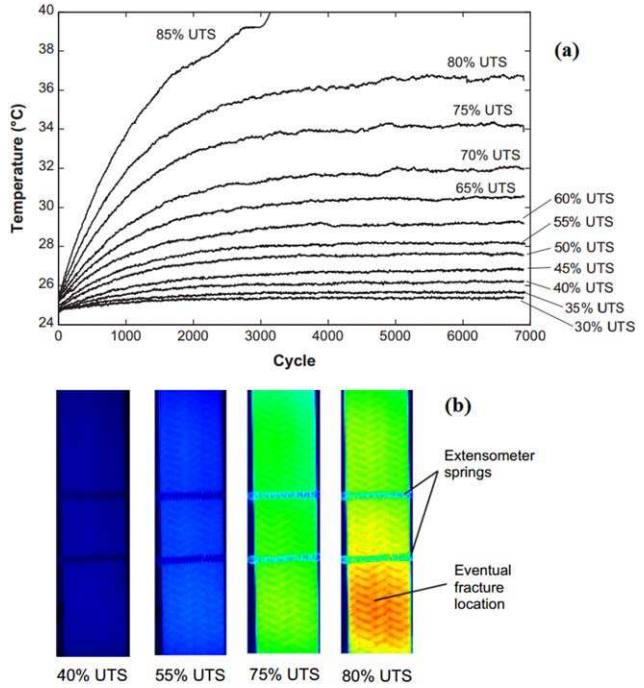

FIG. 15. (a) Temperature variation with change in UTS; (b): Temperature profile at different percentage of UTS [62]. [Color figure can be viewed in the online issue, which is available at wileyonlinelibrary.com.]

reduced. The temperature difference, conversely, was around 10°C when the frequency was increased from 3 to 5 Hz (Fig. 14a). The knitted fabric was less prejudiced by the matrix heating when compared to the woven fabric. However, a slight improvement in the fatigue performance was observed when the temperature increased mildly due to an increment in the matrix toughness with a rise in the temperature (Fig. 14b).

Montesano et.al. [62] did fatigue assessment of triaxially braided carbon fiber fabric in thermosetting polyimide resin by thermographic approach. The thermography measurement technique depends on the use of an infrared (IR) camera to provide a time-dependent contour map of an object's surface temperature, which depends on the energy dissipation when loaded. In PMCs, this energy dissipation occurs due to factors, such as, visco-elastic nature of the matrix, matrix cracking, fiber fracture, and so forth. The use of IR camera is related to the dissipated heat (as a function of temperature), intrinsic energy dissipation and the number of cycles to failure. The experiments were conducted at the stress ratio (R) of 0.1 to the frequency of 10 Hz. It was observed that at lower stress amplitude, the temperature rise was almost constant but it was abrupt at higher stress amplitudes (Fig. 15a). Thermographic images (Fig. 15b) showed constant temperature distribution upto 55% of UTS. However, as the stress amplitude was increased, the difference in temperature distribution was noted. Temperature at the failure region was higher than the rest of the region which proved PMCs temperature contributes toward the material failure.

DOI 10.1002/pc

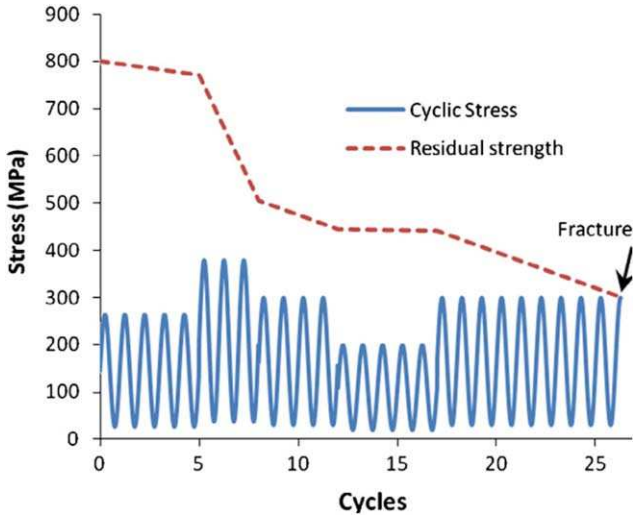

FIG. 16. Strength degradation over number of cycles [25]. [Color figure can be viewed in the online issue, which is available at wileyonlinelibrary.com.]

STRAIN INDUCED, STRENGTH/STIFFNESS DEGRADATION, AND PROBABILITY DISTRIBUTION

Hahn and Kim [63] introduced the concept of the rate of change in residual strength for the evaluation of fatigue results. Residual strength of a composite lamina can be measured in terms of stiffness degradation. It is explained as the loss of stiffness or modulus of a laminate after a certain number of cycles. Stiffness of a composite laminate is always higher in fiber direction as compared to other directions. In this context, Broutman et al. [64] formulated a mathematical model for residual strength in fiber direction, which is:

$$R_{\parallel}^{\mathrm{r}} = R_{\parallel}^{\mathrm{s}} - \sum_{i=1}^{m} \left(R_{\parallel}^{\mathrm{s}} - \sigma_{\max}^{i}\right) \frac{\Delta n_i}{N_{\mathrm{f}}\left(\sigma_{\max}^{i}\right)} \tag{6}$$

where m is the fatigue cycle number in block, Δn_i is the number of fatigue cycles in block i, $R_{\parallel}^{\mathrm{r}}$ is residual strength after m blocks, $R_{\parallel}^{\mathrm{s}}$ is the static fiber direction strength, $\sigma_{\max}^{i}$ is the maximum stress during ith block, N_{f} is the number of cycles to failure in constant amplitude fatigue of $\sigma_{\max}^{i}$.

Kennedy et al. [25] did numerical simulation of the acquired data from the experiments at different stress levels. It was concluded that damage at an early stage is initiated at the initial fatigue loading of the glass fiber laminate. Although the degree of this damage is quite low, nonetheless, its accumulation over a period reduces the capacity of the material to resist stress. The final failure occurs after a considerable number of loading cycles. During experiments, it is not practical to measure the true modulus of the specimen. Instead, secant modulus or fatigue modulus is measured. Figure 16 shows strength degradation over a number of cycles. In this, fatigue modulus is defined as a line which connects maximum stress–strain point to the minimum stress–strain point.

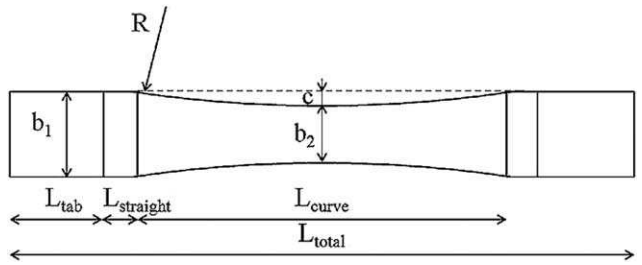

FIG. 17. Dumbbell shaped specimen [65].

Baere et al. [65] studied the TTF behavior of carbon/thermoplastic system and examined the scope of a dumbbell-shaped specimen (Fig. 17). Experiments were conducted at the minimum stress of 0 MPa and maximum stress of 575, 625, 650, and 700 MPa with frequencies of 2 and 5 Hz. The dimensions of the specimen were calculated using different formulae which have been depicted in this article. A structure with $R = 1446$ mm gave the optimum result, which refers to failure occurring at the center of the specimen. The induced longitudinal strain (maximum, minimum, and average) and the number of cycles to failure were plotted (Fig. 18). The center failure pullout cracks were noticed near the tabs. At higher stress levels, less influence of the loading frequency on the fatigue life was observed.

Whitworth [52] proposed stiffness degradation model for composite laminates under fatigue loading in graphite/epoxy laminates. The limitation for his model was with regard to the constant amplitude fatigue loading of the sample. Also, it was assumed that stiffness is a proportionally decreasing function of the fatigue cycles. The residual stiffness is in the form of

$$\frac{dE^*(n)}{dn} = \frac{-a}{(n+1)E^*(n)^{m-1}} \tag{7}$$

where $E^*(n) = E(n)/E(N)$ is the ratio of residual stiffness to failure stiffness, n is the number of cycles, a and m are

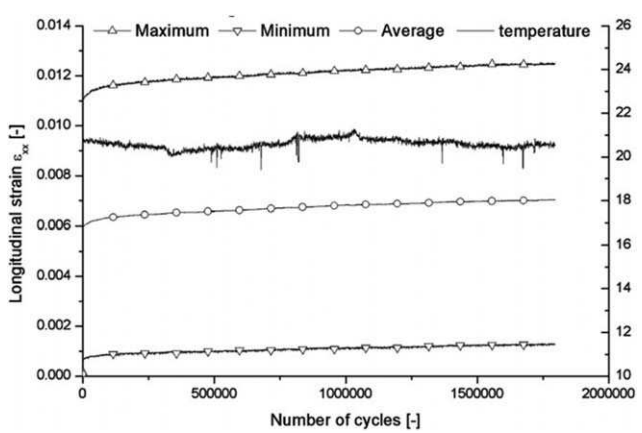

FIG. 18. Longitudinal strain versus number of cycles to failure [65].

parameters depending on applied stress, loading frequency, and environmental condition. Integration of the above equation from 0 to n gives the residual stiffness degradation after n cycles, which is:

$$E(n)=E(N)\left[-h\ln(n+1)+\left(\frac{E(0)}{E(N)}\right)^{m}\right]^{1/m} \quad (8)$$

where $h = a \times m$. $E(N)$ cannot be calculated until the material fails. Thus, failure strain criterion can be introduced, according to which, failure will occur when the failure strain reaches the ultimate tensile strain, that is

$$\frac{S}{S_u}=C_1\left[\frac{E(N)}{E(0)}\right]^{C_2} \quad (9)$$

The above equation has related the ratio $^{E(N)}/_{E(0)}$ to the ultimate strength (S_u) and the applied strength (S) using constants C_1 and C_2, which could be found out experimentally. Using all the parameters and equations and putting them in Equation *8*, one gets the equation for residual stiffness $E(n)$ as;

$$E(n)=E(0)\left(\frac{S}{C_1S_u}\right)^{1/c_2}\left[-h\ln(n+1)+\left(c_1\frac{S_u}{S}\right)^{m/c_2}\right]^{1/m} \quad (10)$$

To support the mathematical model, experiments were conducted on 30 samples with loading stress of 80, 70, 60, 57.5, 55, 52.50, 50, 47.50, 45, and 40% of the ultimate tensile stress of the specimen. Test results above 60% of the ultimate tensile stress were too inconclusive for further consideration. The modulus reduction ratio was plotted against fatigue cycles at 57% of the ultimate strength of the material.

Philippidis et al. [66] did a comparative study on the theoretical and experimental residual strength of the carbon-epoxy and glass epoxy composites after their fatigue testing. Their investigation dealt with probabilistic and deterministic models of the strength degradation under various loading conditions. Models which were numerically investigated were Broutman and Sahu, Harris et al. (INT), Hahn and Kim (H), Various (REI), Philippidis and Passipoularidis (OM), Sendeck (W1, W2), and Yang et al. (Y1 and Y2). Experiment data were collected from different literature, presented by Yang [67], Anderson et al. [68] and Philippidis et al. [69]. Predictions of the residual strength distribution, based on these literature, were plotted. Cumulative distribution function or probability distribution function was plotted against the residual strength. Figure 19 shows probability distribution function of residual stress as presented by Yang [67], Fig. 20 shows strength degradation over cycles as studied by Anderson et al. [68] with the help of different strength degradation theories, Figs. 21 and 22 show strength degradation over a number of cycles at different stress levels and probability distribution of different stress levels respectively, as investigated by Philippidis et al. [69]. All the figures referred above have been published by Philippidis et al. [66].

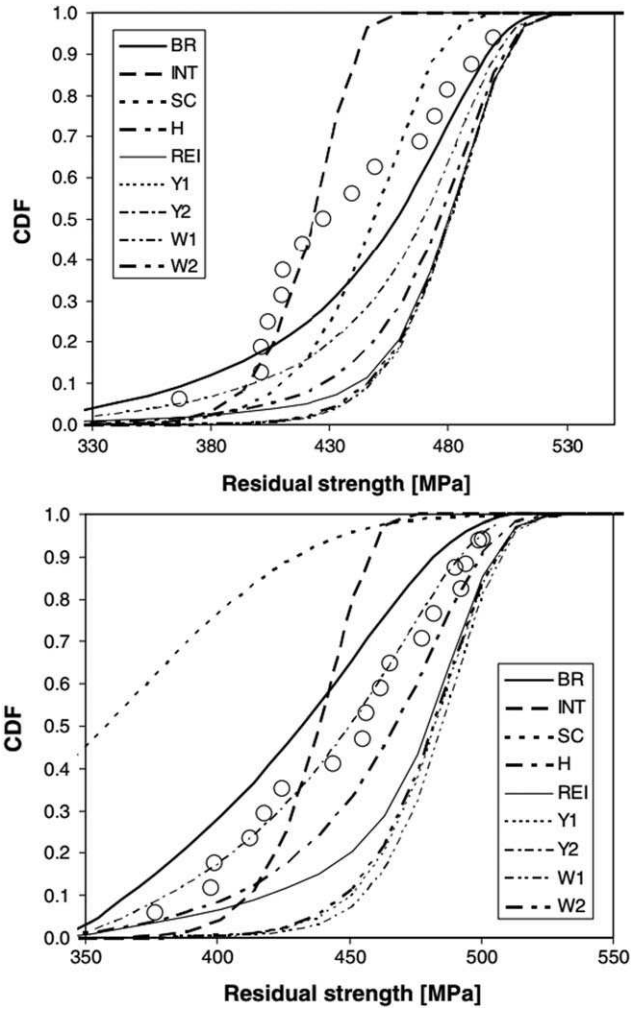

FIG. 19. Probability distribution of residual strength by different models [66, 67].

CYCLIC BEHAVIOR

Cyclic stress strain curve or hysteresis curve is a common method to describe cyclic loading behavior of a material. This curve is drawn using a set of stabilized hysteresis loops at different strains. The area bound by hysteresis loop shows loss of stiffness in the respective cycle. In 1986, Hwang et al. [70] presented the fatigue aspect of a composite, based on the fatigue modulus concept. In fatigue loading of a composite stress–strain diagram, changes as degradation of the composite take place with every cycle. The fatigue modulus of every cycle can be calculated accordingly as it is a function of applied stress and the number of cycles provided at the end points are available, which can be obtained by conducting experiments. Figure 23 shows hysteresis curve.

DOI 10.1002/pc

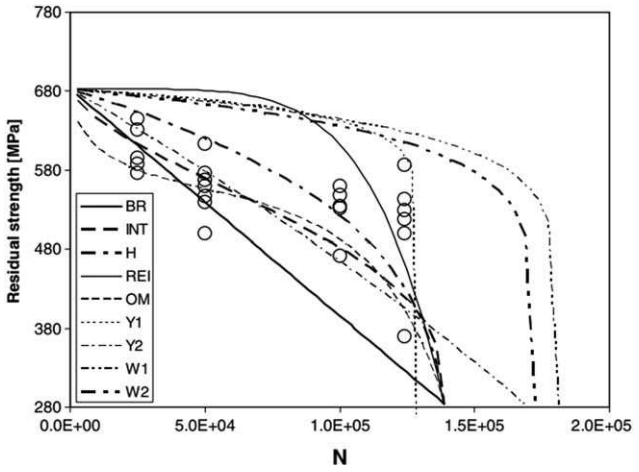

FIG. 20. Strength degradation over number of cycles by different strength degradation theories [66, 68].

In this context Brunbauer et al. [17], [71] studied the cyclic behavior of carbon fiber reinforced polymer composites under quasi-static and TTF loading. In their investigation, Brunbauer and Pinter [71] used different strain measurement techniques, such as, strain gauges, mechanical extensometers, digital image correlation (DIC), and 2D camera systems. The results were compared with the strain measured by servo-hydraulic piston. Like other local strain measuring instruments, the strain measured by the piston was applicable not only to the test sample but to the entire system, including the testing machine, which gave additional data for the fatigue test. The maximum static modulus and dynamic modulus were calculated from the static stress–strain and hysteresis curve respectively, as follows:

$$E_s = \frac{\sigma_{max}}{\varepsilon_{max}} \tag{11}$$

$$E_{dyn} = \frac{\boldsymbol{\sigma_{max} - \sigma_{min}}}{\boldsymbol{\varepsilon_{max} - \varepsilon_{min}}} \tag{12}$$

To effectively find out the strains, different strain measuring tools were fixed on the samples. For example, one sample was fitted with four strain gauges, two in front and two at the back of the sample, to find out strains in transverse and longitudinal direction of the applied load together with an optical strain measuring instrument and extensometer. Another sample was fitted with DIC and extensometer in the front and two strain gauges at the back. During the fatigue test, hysteresis shifted toward higher strains with an increase in load cycles, irrespective of the method deployed to measure the strains. Hysteresis measured by extensometer was steep and slender which proved the least deviation when strains were less than 0.3%. Conversely, those measured by piston displacement had fewer slope but possessed narrow shapes. Moreover, when measured by strain gauges, strains shifted to more than 0.25% and had wider shape which could not be related to UD 45°. For all layups (0°, 45°, 60°, 90°, and ±45°), stress–strain hysteresis recorded by extensometer and hydraulic piston was used for moduli calculations. Dynamic modulus measured was higher than quasi-static modulus in terms of all parameters. Dynamic modulus measured using piston and extensometer showed constant decrement of ±45°, while for UD 45°, it remained constant or even increased. For UD 90°, it remained constant showing no fiber movements or damage increment till a sudden failure.

Knoll et al. [20] studied the hysteresis behavior of the specimen in tension–tension ($R = 0.1$) and tension–

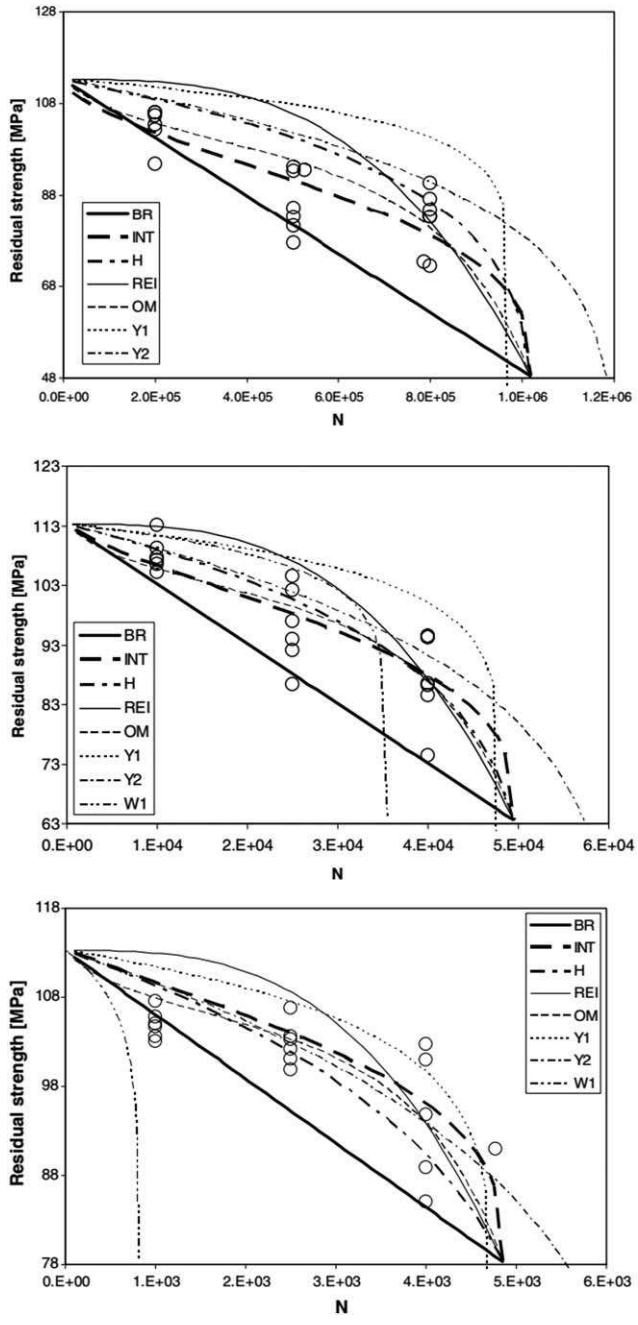

FIG. 21. Strength degradation over number of cycles at different stress levels [66, 69].

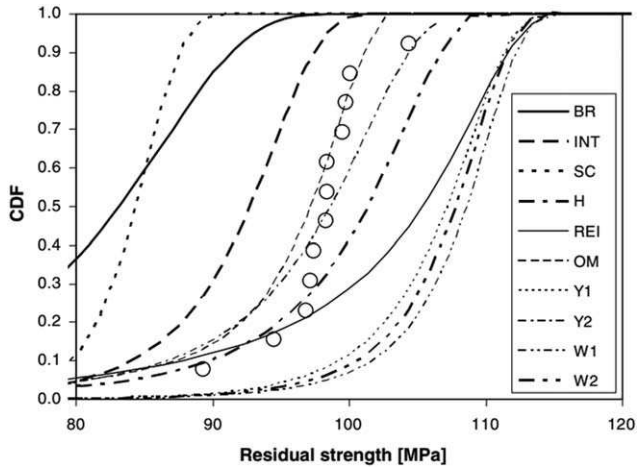

FIG. 22. Probability distribution for residual strength by different models [66, 69].

compression ($R = -1$) fatigue test for composites with different fiber orientations and fiber volume fraction. The last hysteresis in tension–tension loading shifted toward high strain, witnessing progressive damage during the last cycles. fiber pullout was considered to be the main reason for this behavior. However, the shape of hysteresis did not change at any strain level. In tension–compression fatigue, the hysteresis behavior was different. For the last few cycles, the loop shifted toward the high strain zone in tension but stayed near the low strain zone in compression. The fiber pullout during tension together with fiber interference during compression was considered to be the main reason behind this behavior. The same performance was witnessed in the composite with unidirectional 45° fiber but for laminate with 0° fiber angle, the stress–strain curve overturned during the T–C test. Continuous expansion of fiber fracture was held responsible for this behavior of the hysteresis loop.

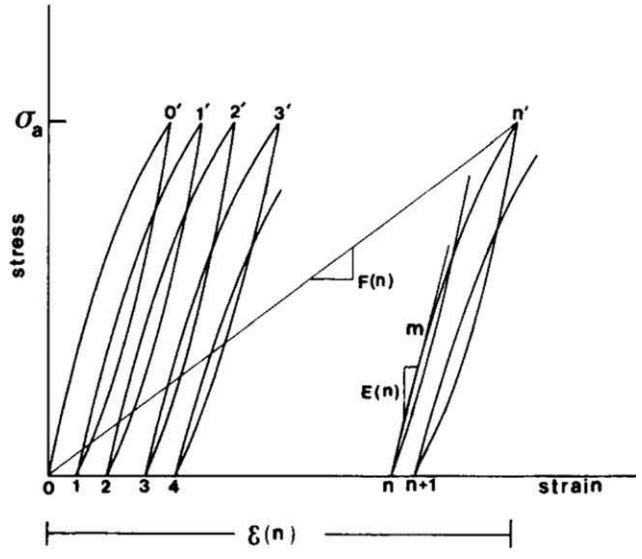

FIG. 23. Cyclic stress–strain curve or hysteresis curve [70].

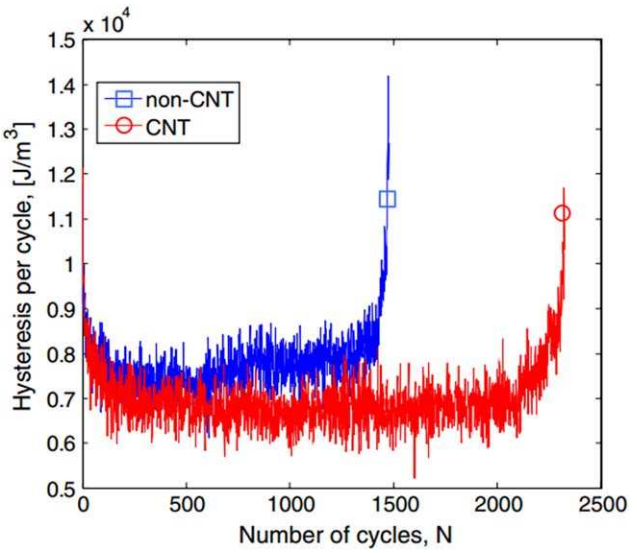

FIG. 24. Adding CNTs increases hysteresis effectively which in turn increases fatigue life [37]. [Color figure can be viewed in the online issue, which is available at wileyonlinelibrary.com.]

In this context, Grimmer et al. [37] studied the high cycle fatigue behavior of the CNT modified glass fiber - epoxy composite. As far as the static behavior of the samples was concerned, there was nominal difference between the ultimate strength of the epoxy with and without CNT. However, epoxy with CNT failed at a higher strain. For the same amplitude of stress, the fatigue cycle increased in the laminate with 1% CNT. Addition of 1 wt% of CNT improved the hysteresis effect by almost 60%, thus increasing the number of cycles to failure. The energy loss was low in CNT modified matrix, resulting in a decreased stiffness loss (Fig. 24).

NOTCH/STRESS CONCENTRATION

Taking account of the notch or stress concentration is an important factor in the designing of fiber reinforced polymer matrix composites as failure always starts at the point of stress concentration and it may also lead to rapid propagation of the crack. As no product is perfect, it is, therefore, always a good idea to make an allowance for the failure. In this regard, Mar-Lin [72] proposed a model for fracture mechanics correlation for tensile failure in filamentary composites with holes. Unlike metal, composites are heterogeneous in nature and a uniform model for the fracture behavior cannot be applied to them. The Mar-Lin model can be expressed as:

$$\sigma_N^{\infty} = \frac{H_c}{(2a)^{mY}} \tag{13}$$

where σ_N^{∞} is residual strength, H_c is composite fracture toughness, $2a$ is notch length, m is order of stress singularity, and Y is geometry factor.

The effect of stress concentration on the fatigue behavior of a composite has been studied by a number of

DOI 10.1002/pc

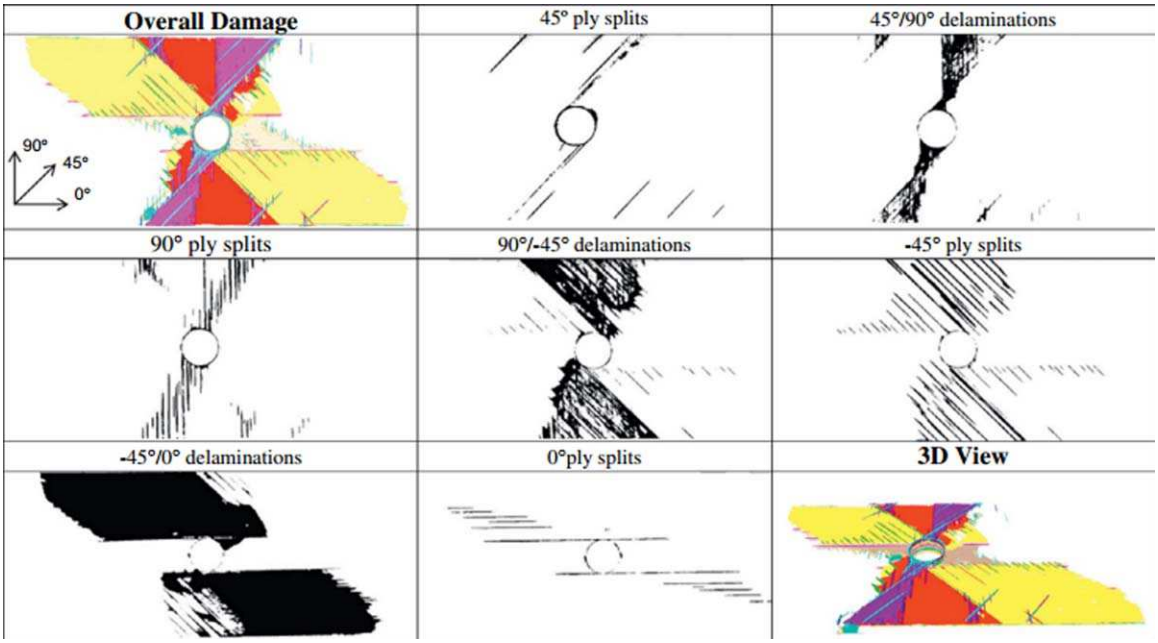

FIG. 25. X-ray CT slice of the specimen under interrupted fatigue test with 14% stiffness loss. [26]. [Color figure can be viewed in the online issue, which is available at wileyonlinelibrary.com.]

researchers. Nixon-Pearson et al. [26] carried out the TTF test on carbon/epoxy laminated specimen with a central hole of 3.175-mm diameter. The tests were carried out at a constant amplitude with $R = 0.1$ and frequency of 5 Hz. Each test was performed upto 10^6 cycles or 15% loss in stiffness, whichever came earlier. Different damage phenomena were observed around the free edges of the hole. Matrix cracking, debonding and delamination started from the hole. To find out the 3D failure order of damage using X-ray Computed Tomography (CT), interrupted tensile tests at 60 and 80% of the ultimate strength as well as fatigue tests at 60% of the ultimate static strength were carried out. X-ray images of the sample loaded at 40% of the ultimate strength and after 10^6 cycles revealed very nominal damage. Matrix cracking of the 90° plies next to the split, little matrix cracking of −45° plies, and splitting of the surface plies and 0° plies were observed as major damages. Selective samples went under interrupted fatigue tests to assess the damage development with different stiffness loss of 4, 14, and 50%, respectively. At the starting, secluded splits were observed which then started to join up to form a triangular delamination region between the plies of +45° and 90°. Asymmetric −45/0 delamination caused drop in effective modulus. This can be termed as the dominant failure incident. Figure 25 shows X-ray CT slices of the interrupted fatigue tests for the laminate with 14% stiffness loss.

Bizuel et al. [31] studied the fatigue crack growth in thin notched sample of woven glass fabric under tensile loading. Samples were 30 and 50 mm in width. Growth of cracks was studied in both warp and weft direction of the fabric. Laminates in the weft direction took longer cycles for crack initiation as compared to warp direction as the matrix damage took place earlier in the weft direction. From Fig. 26a and b, one can observe that crack growth is rapid in nature, irrespective of the sample width and crack propagates perpendicular to the yarn fabric.

Broughton et al. [73] studied the behavior of open hole GFRP laminate in TTF. DIC and multiplexed fiber Bragg grating (FBG) sensors were used and their applicability in the strain monitoring was also evaluated. The FBG sensors remained intact and responsive till the test was concluded. When applying strain gauges, the FBG sensors, conversely, showed grid failure and became insensitive over prolonged testing at low and high amplitude. During the tests, the DIC system was used to obtain 2D maps of the strain distribution within the samples. During the open hole tension fatigue test, a hole of 6mm diameter was drilled using water cooled tungsten carbide tool setup. End tabs were not used as it was assumed that failure will occur at the center due to high stress concentration in this area. Experiments were conducted at a constant amplitude and with $R = 0.1$ and 0.5. The S–N plot used linear regression lines of the best fit. Three stages were observed in residual stiffness degradation curve at different stress levels, which were; (I) rapid decrement in stiffness, generally caused by matrix cracking between 45° and 90° plies, (II) gradual stiffness reduction due to additional ply cracking within all plies and delamination at the interfaces between 45° and 90° plies, and, (III) failure of samples due to accumulation of delamination, ply cracks and debonding. The failure occurred at the center of the laminate as assumed.

Aidi et.al. [74] studied the fatigue life of centrally notched, quasi-isotropic, carbon/epoxy laminate. DIC, radiography, non-contact vibration measurement techniques

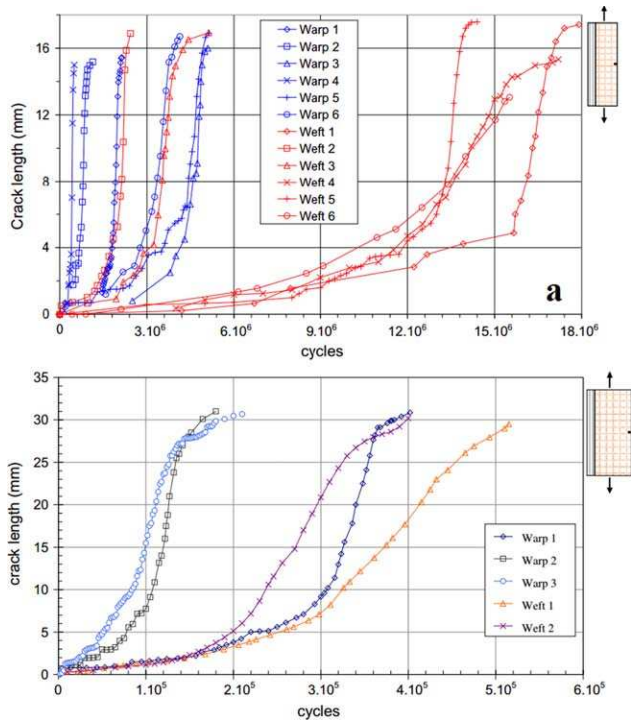

FIG. 26. Fatigue crack growth is rapid and crack propagation is independent of specimen width [31]. [Color figure can be viewed in the online issue, which is available at wileyonlinelibrary.com.]

were used to harness the residual characteristics and corresponding damage states in the laminate and X-ray CT was used to measure the extent and location of damage within the samples. Fatigue tests were conducted at the frequency of 10 Hz and stress ratio (R) of 0.5 till the final fracture or upto 10^6 cycles, whichever occurred first. While DIC was used to plot the 2-D contours of the strain (ε_{xx}, ε_{yy}, and ε_{xy}) around the stress concentration in quasi-static and fatigue tests, Laser doppler vibrometry was used to measure vibration velocity and displacement of the sample without its loading and to evaluate the fatigue damage evolution by the residual frequency response functions of the notched composite. X-ray CT was used to track the fatigue damage pattern by discontinuing the fatigue tests in between. DIC was used successfully to plot the magnitude (Fig. 27a) and contours (Fig. 27b) of the strain against the normalized distance from the hole at various life fractions of the fatigued samples. The maximum axial strains were observed in the perpendicular direction to the loading while the minimum axial strains were observed in the parallel direction to the loading. Integrated 3-D image of the sample showed four modes of damage. Starting from the point of their occurrence, these modes were; transverse cracking at 90° plies, offset cracking in ±45° plies, axial splits tangent to the hole and delamination in the interface between the plies. Post fatigue, quasi-static tests on laminates revealed 13.6% increase in residual strength as compared to unfatigued laminate. This was due to splitting at the hole edges, which caused blunting of the notch.

Fatigue testing of fiber reinforced composites is always carried out with the use of end tabs to offset the effect of failure in grips which hampers both the result and the experiment setup. ASTM D3039 [75]/D3479M [76], which prescribed the standard method for quasi-static and fatigue testing of fiber reinforced composites, respectively, have recommended the use of end tabs. It suggests that the length of the tabs should be 50 mm and it should hang 10 mm out of the grips. When loaded statically or dynamically, the material must fail within the gauge length or in the zone where perceptively stress concentration is greater so as to assess the failure mechanism [77]. Failure is unacceptable in or near the tabs or even in the grips where there are no tabs. Thus, it is very important to understand the use of tabs to get valid results. In this context, Baere et al. [78] worked on the design of end tabs for both quasi-static and fatigue testing of fiber reinforced polymer for mechanical clamps and hydraulic clamps.

Investigations were carried out on four different tab materials and tab geometries. Different tab geometries can be seen in Fig. 28. Tab materials inspected were glass/epoxy, aluminium, PPS, and steel. For each setup, aluminium shows the highest stress concentration whereas glass/epoxy and PPS show the lowest stress concentration. Higher stress concentration leads to the failure of the specimen in that area. For the right result, it is mandatory for the failure to occur at the center of the specimen and not anywhere else although failure occurring at the end of the tabs is also acceptable.

MULTIAXIAL STRESS

Multiaxial stress is present in many structures. Presence of multiaxial stress in uniaxial loading can be due to irregularities and stress concentrations. Amijima et al. [79] studied the multiaxial fatigue behavior of woven glass fabric under torsion-tension loading in tubular and dumbbell-shaped specimen. Tapered end tabs were added to remove stress concentrations. Axial and torsional loads were applied simultaneously at the room temperature. For several stress ratios or biaxiality ratios (axial stress/shear stress) (Fig. 29), static failure strength under monotonically increasing biaxial stress was observed. Effect of initial length, initial tension together with the effect of surface smoothening of the specimen, were studied as well. Biaxial tension–torsion fatigue life of the specimen highly depends on the stress ratio or biaxiality ratio, that is, axial stress/shear stress. The fatigue life of the specimen was higher when stress ratio was 4:9 compared to the stress ratio of 1:1 (Fig. 30) because for stress ratio 1:1, cyclic shear stress component was higher compared to the stress ratio of 4:9. Thus, one can conclude that the fatigue life degradation does not follow linear relation with the biaxial stress ratio.

Kawakami et al. [80] studied the biaxial fatigue loading of glass fiber cloth reinforced polyester composite.

 DOI 10.1002/pc

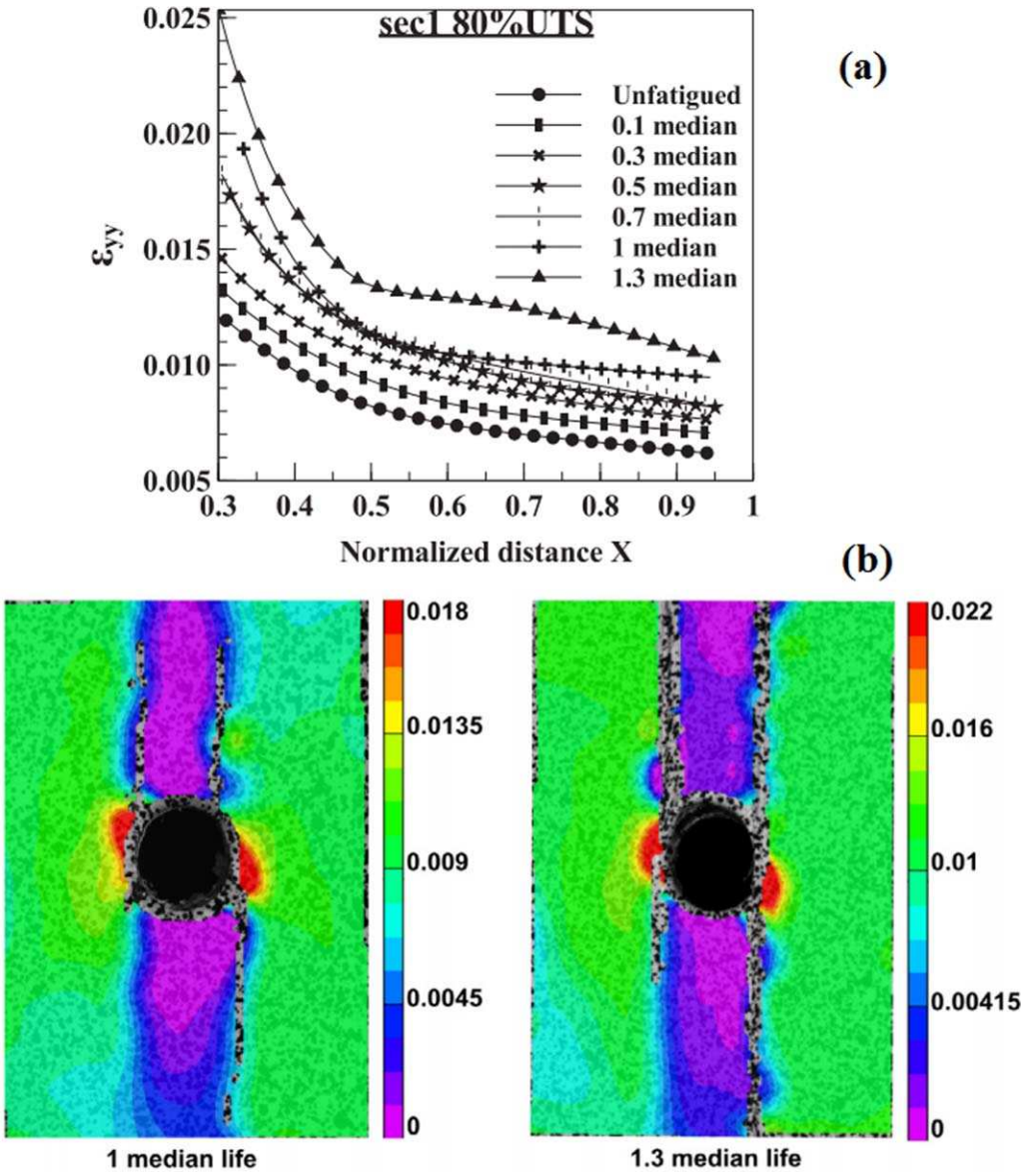

FIG. 27. (a) Full field longitudinal strain profile at 80% of the UTS for different fatigue life; (b): Full field longitudinal strain counters at 80% of the UTS at 1 and 1.3 median life [74]. [Color figure can be viewed in the online issue, which is available at wileyonlinelibrary.com.]

The study was carried out at five different stress ratios/biaxiality ratios (i.e., axial stress/shear stress) of 1/0, 7/1, 3/1, 1/1, 0/1. Testing frequency was of 2 Hz with temperature at 296 K and 60% humidity. Stress ratio of 3:1 meant that for three cycles of axial load, one cycle of torsional load was applied. Effect of the loading path on the fatigue behavior of the specimen was studied. The loading path was found to have no significant effect on the fatigue behavior although slope of the S–N curve decreased with a decrease in the biaxial stress ratio, demonstrating modulus decays with an increase in loading cycles. Pure torsion had a remarkable effect on the fatigue life of the specimen as the critical damage level in pure torsion was 0.53 as compared to 0.30 of pure axial loading. Also, fatigue damage under pure torsional loading moved along transverse as well as longitudinal direction.

Fuji et al. [81] studied the effect of notch sensitivity of the glass fiber woven fabric with a circular hole under the biaxial tension–torsion loading at five different stress ratios (axial stress/shear stress) of 1/0, 7/1, 3/1, 1/1, 0/1 under room temperature and laboratory condition. For each experiment, the biaxiality ratio was kept constant. Figure 31 shows the specimen dimension. Comparative S–N curves for different stress ratios of the notched and unnotched specimens were plotted. The notched specimen showed degraded fatigue life as compared to unnotched specimen. Rapid decrement in the strength of the specimen under axial loading and a gradual decrement in the same specimen under the pure torsion loading was noted.

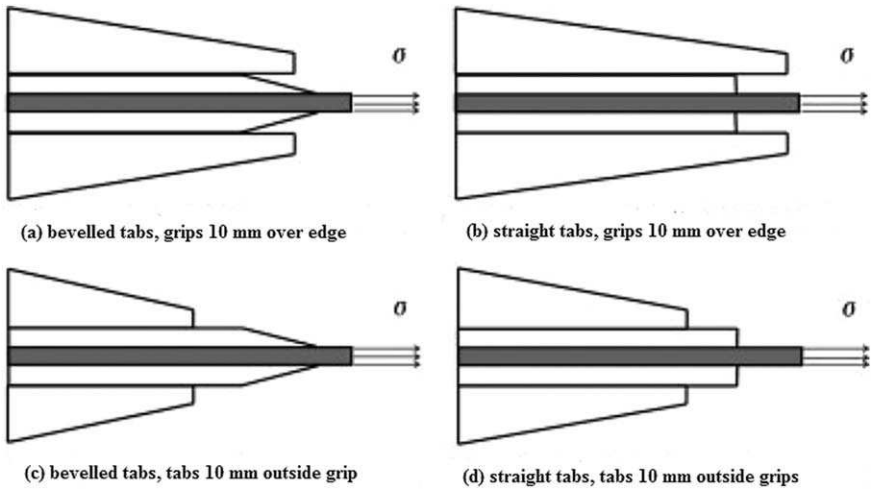

FIG. 28. Tab design [78].

A sharp decline in the strength was observed for the biaxiality ratio of 1:1. Apart from this, under biaxial loading, when the tensile stress component was large, fatigue notch factor decreased with an increase in the fatigue life. Conversely, the fatigue notch factor increased when the shear stress component was large.

ENVIRONMENTAL EFFECT

Most of the components that are made of composite materials for using in adverse external conditions, which is way too removed from the conditions in which they are tested. In general, the majority of the tests on the laminates are carried out in laboratory condition while ideally an aeroplane, made of these materials, has to work in cryogenic temperature. Similarly, materials, used in ship building, have to be tested under moisture and saline condition which degrades the physical properties of the material.

Temperature Effects

Polymer composites are viscoelastic materials and their properties largely depend on the working temperature. Rise in temperature upto the degree of glass transition temperature (T_g) leads to reduction in strength, modulus and fatigue life. Jen et al. [82] worked on the samples made of graphite/PEEK (AS-4/PEEK) prepreg with different layups of $[0/90]_{4s}$ cross ply and quasi-isotropic $[0/45/90/-45]_{2s}$ laminates with 61% of fiber volume fraction. Fatigue tests were carried out at a stress ratio of $R = 0.1$ and frequency of 5 Hz. The reported glass transition temperature for the PEEK was 416 K. The experiments were conducted at room temperatures (25°C, 75°C, 100°C, 125°C, and 150°C) for 10^6 cycles. It was concluded that at the highest testing temperature, strength is the lowest. Moreover, cross ply laminates have better properties than the quasi-isotropic laminates and fatigue tests at or near the T_g degrades material properties rapidly. The S–N curve for cross-ply and quasi-isotropic laminates at different temperature is shown in Fig. 32a and b.

Kawai and Taniguchi [83] worked on the off-axis fatigue behavior of the carbon/epoxy system at room and elevated temperatures of 100°C. Samples with five different fiber directions, that is, at 0°, 15°, 30°, 45°, and 90°, were used for testing. TTF tests were carried out upto 10^6 cycles at $R = 0.1$and at frequency of 10 Hz with sinusoidal waveform. The axis fatigue strength for a given life

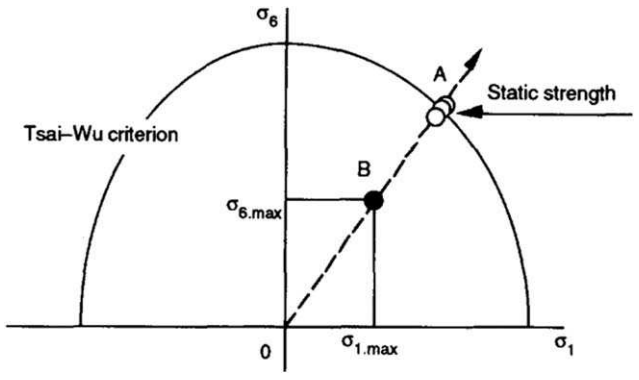

FIG. 29. Stress ratio under biaxial loading [79].

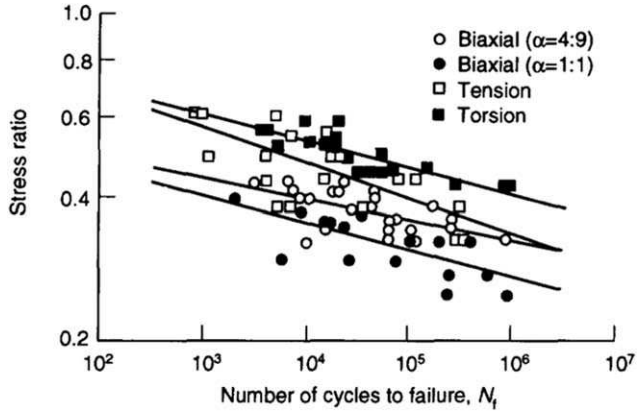

FIG. 30. S–N curve at different biaxiality ratio [79].

DOI 10.1002/pc

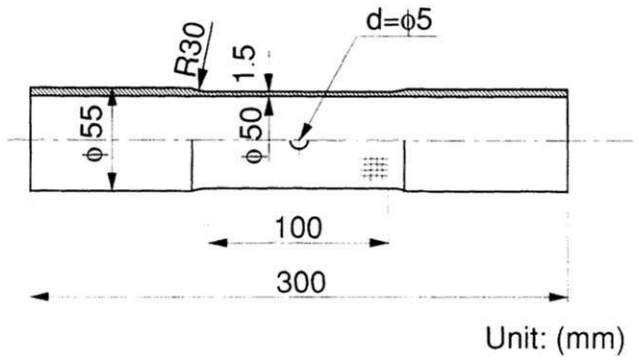

FIG. 31. Notched specimen dimension for biaxial fatigue tests [81].

of 10^6 cycles was found to be as high as 80% of σ_u, while off-axis tests at 15°, 30°, and 45° showed high sensitivity toward fatigue as the S–N curve got steeper during the intermediate cycles. With widening of the off-axis angle, fatigue strength decreased as well. At a higher temperature, the fatigue limit turned out to be low. However, as far as the shape of the S–N curve and fiber orientation were concerned, the trend remained the same as that of the room temperature. The fatigue failure pattern at room temperature was also similar in appearance to that of the static tensile failure pattern at 100°C. In the on-axis specimen, no difference in failure was detected either for static tensile or for the T–T fatigue test.

Rotem et.al. [85] developed a fatigue failure criterion for fiber -based composite and applied it to predict the fatigue life of graphite/epoxy laminates at different temperatures. The strain–stress curve for tensile tests and S–N curve for TTF test were generated for unidirectional (10°, 15°, 30°, 45°, 90°) angle ply (±15°, ±30°, ±45°, ±60°, ±75°) and symmetrically balanced laminates ($[0°/\pm15°/0°]_s$, $[0°/\pm30°/0°]_s$, $[0°/\pm45°/0°]_s$, $[0°/\pm60°/0°]_s$, $[0°/\pm75°/0°]_s$, $[0°/\pm90°/0°]_s$) at 25°C, 74°C, and 114°C temperatures. For most of the laminates, reduction in static and dynamic strength was observed with an increase in the temperature. Reduction was more emphatic in dynamic loading, especially where the shear stress was more dominant. For UD 0° plies, static strength did not get affected with a rise in temperature as properties were fiber dominated, while angled UD plies showed variation in properties, resulting in a theory that angled plies are matrix-dependent. For 90° plies, properties were so low that there was hardly any variation in properties with change in the temperature. Angled plies failed due to in-plane shear which led to propagation of the first crack through the matrix across the specimen as these plies were dominated by matrix properties. Laminates with lower angles were observed to have very low in-plane shear and transverse stress, which led them to fail by delamination rather than by in-plane shear stress. The UD lamina, loaded in the fiber direction, showed high fatigue strength, independent of the applied cycles. There was no temperature dependency as properties were fiber-dependent. Moreover, in the case of static testing, temperature had no significant effect on the strength. For angled plies, properties were matrix-dependent. Therefore, temperature and off-axis load showed negative effect on the fatigue strength. In symmetrically balanced laminates, predictions were made for the failure mechanism and the experiment agreed with the predictions made. $[0°/\pm15°/0°]_s$ laminate failed by delamination of ±15° plies, which was in accordance with the prediction. Conversely, $[0°/\pm30°/0°]_s$ failed by in-plane shearing of ±30° plies as predicted and $[0°/\pm90°/0°]_s$ failed by the fatigue failure of 0° plies as 90° plies did not contribute much to the strength of the laminate.

Shindo et al. [40] studied the fatigue behavior of plain weave glass/epoxy composite under tension–tension

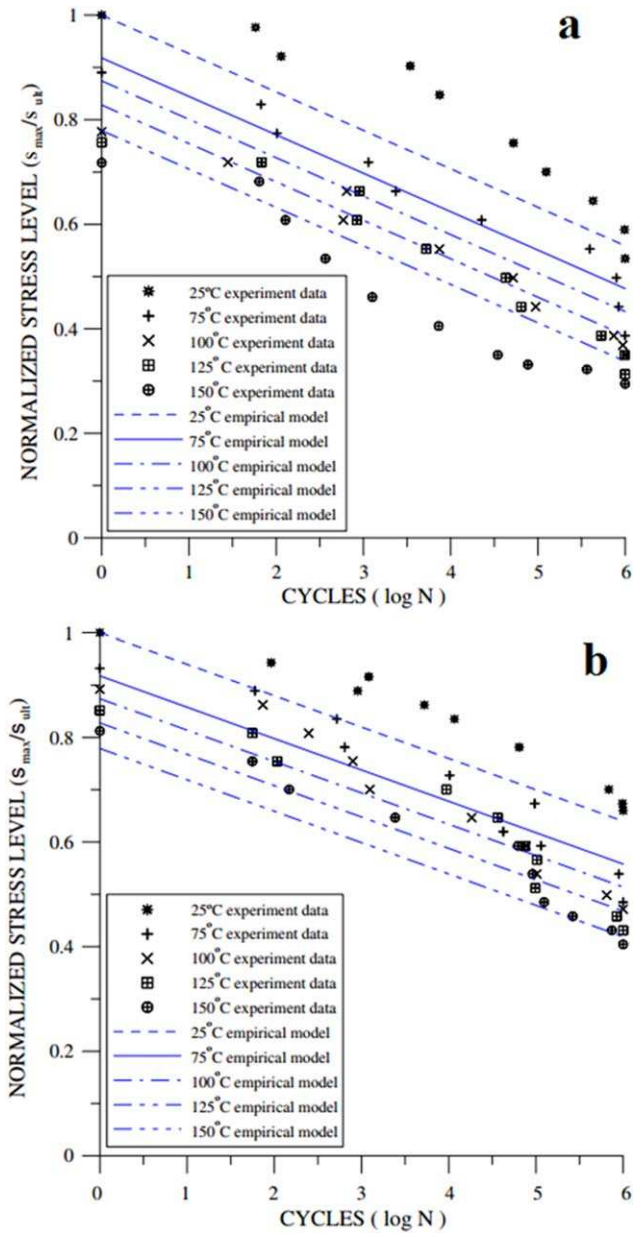

FIG. 32. Wohler curve for (a) cross ply and (b) quasi isotropic laminate at different temperatures [82]. [Color figure can be viewed in the online issue, which is available at wileyonlinelibrary.com.]

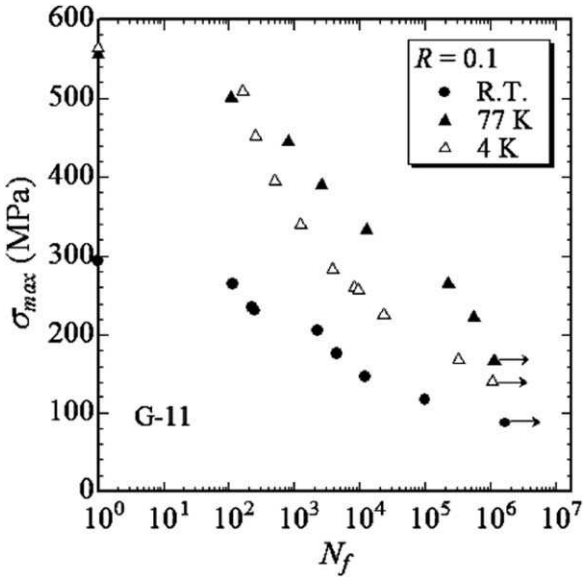

FIG. 33. S–N plot for plain weave glass/epoxy laminate at room and cryogenic temperature [40].

loading at cryogenic temperature. TTF tests were conducted at the frequencies of 4 and 10 Hz with stress ratio of 0.1. Experiments were conducted at room temperature, that is, 77 K and 4 K. Fiber volume fraction of the laminates was reported to be 47%. Cryogenic test conditions were achieved by submerging the coupons and loading apparatus in liquid nitrogen and liquid helium, respectively. Ultimate stress was reported to be twice that of the room temperature. Knee point was seen during the monotonic loading of the samples, showing change in modulus of the laminate, which was 264 MPa at 77K and 256 MPa at 4K. Figure 33 showed the S–N curve comparing the fatigue property of the laminate at room temperature and cryogenic temperature. Although static strength of the composite was higher at 4K as against 77K, samples at lower temperature (4K) survived less numbers of cycles when compared with samples at comparatively higher temperature (77K). No explanation can be given regarding this phenomenon. The number of cycles to failure was observed to be reducing by a small quantity but loading capacity was enhanced.

Takeda et al. [24] studied the effect of cryogenic temperature on epoxy matrix, modified with 0.5 wt% MWCNTs, and, *n*-butyl glycidyl ether (BGE) on the cryogenic temperature. Four different samples with different constituents were made: (a) laminate with neat epoxy, (b) laminate with 0.5 wt% CNT, (c) laminate with 10 phr BGE, and (d) laminate with 0.5 wt% CNT and 10 phr BGE. Static and cyclic tensile tests were conducted at 77K temperature while the stress ratio was at 0.1 and loading frequency was at 5 Hz. An increment in modulus and formation of knee point (it is a sign of damage accumulation) were reported when MWCNT was added. However, slight decrement in the ultimate tensile strength was observed on adding MWCNTs. The fatigue test was carried out at 60% of the ultimate strength. Samples modified with MWCNTs and BGE showed slight increment in fatigue life when compared with unmodified samples. However, the fatigue life of the samples with both MWCNTs and BGE increased significantly. Increment in the matrix-based mechanical properties was reported after matrix modification with the nano particles. MWCNTs and BGE were found to be very effective in damage suppression as these nanoparticles arrest damage propagation and in fatigue testing a lot of energy get dissipated to overcome these hindrances. Figure 34a and b show the difference in properties at 77K temperature after adding different materials to modify matrix.

Moisture Effect

Of late, greater emphasis has been laid on the hygrothermal behavior of materials. Application of heat together with moisture generates hygrothermal condition. Moisture has a deep impact on the physical, chemical, and mechanical properties of glass fibers as these fibers are more sensitive to hygrothermal ageing as compared to carbon fibers. Moisture affects the fibers, matrix and interfaces in different ways. In this context, Hu et al. [85] studied the effect of hygrothermal ageing on the fatigue of glass fiber/poly dicyclopentadiene composites.

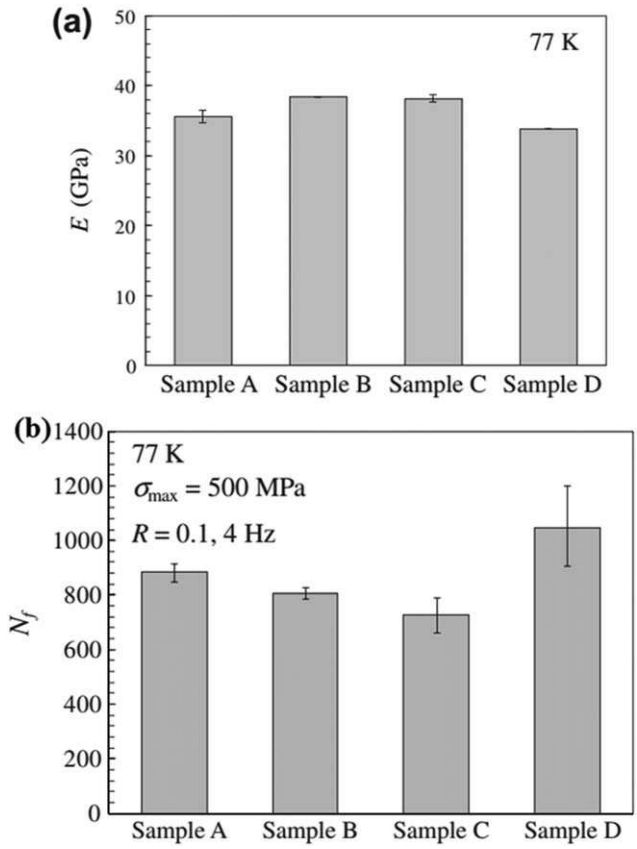

FIG. 34. (a) Young's modulus of samples modified with different materials at 77K; (b): Decrement in fatigue life at cryogenic temperature after adding 0.1 wt% of CNTs [24].

DOI 10.1002/pc

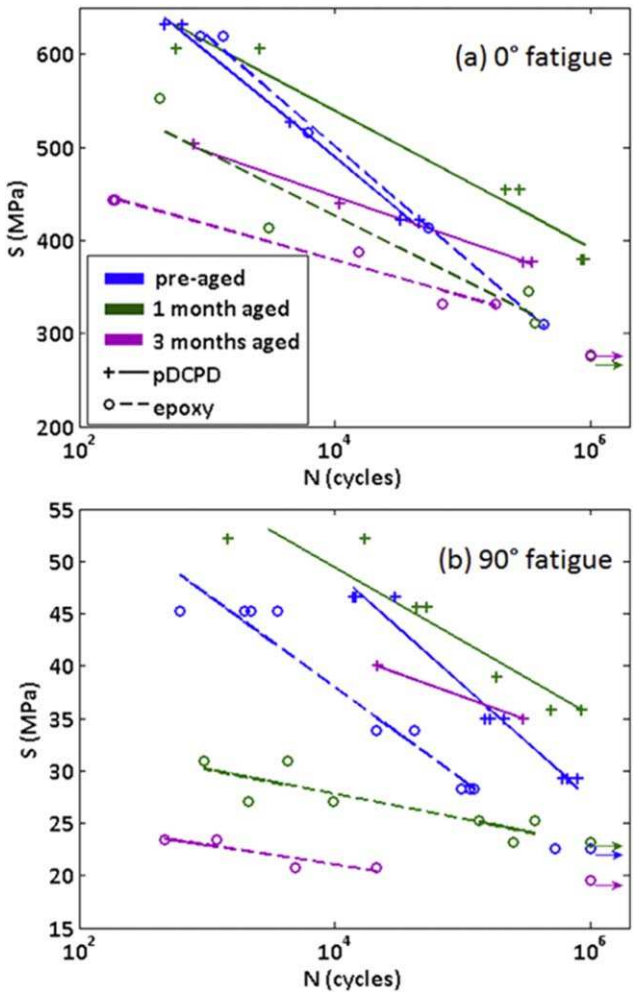

FIG. 35. S–N curve of aged and unaged samples when loaded in (a) warp and (b) weft direction [85]. [Color figure can be viewed in the online issue, which is available at wileyonlinelibrary.com.]

Deionized water and salt water at 60°C were used as submersion medium and glass/epoxy composite was used as the datum for comparison of results. Samples were tested for change in weight in the intermittent period. Fatigue tests were carried out at stress ratio (R) of 0.1, frequency of 10 Hz and runout cycles of 10^6. Results showed that the aged samples could not last till the runout cycles. Figure 35a and b show the S–N curve at the warp and weft direction loading in the aged and unaged samples. In TTF of 0° fiber, one month old samples withstood greater stress due to the strengthening of matrix by ageing and/or post curing. Conversely, in the same TTF with 90° fiber, where matrix properties are more dominant rather than fiber properties, one month old samples showed increased stress-bearing capacity due to superior interface adhesion and/or matrix strengthening.

Selzer et al. [86] studied the effect of moisture on mechanical properties of carbon fiber reinforced polymer composites. Unmodified and modified toughened epoxy thermoset matrix and one thermoplastic matrix were used in this investigation. Three different orientations, that is, $([0]_{16}$, $[90]_{16})$, $([0, 90]_{4s})$, and $([0, \pm 45, 90]_{2s})$, were used in the present study. The samples were placed in distilled water at 23°C, 70°C, and 100°C of temperatures to let them absorb the moisture. In between, the samples were removed from the bath to note the change in their weight. The process was repeated until reaching the saturation point. Fatigue tests were conducted with the stress ratio of $R = 0.1$, frequency of 10 Hz and load of upto 2×10^6 cycles. The S–N curve for carbon fiber laminate was flat proving that carbon fiber has good fatigue life. When loaded in fiber direction, the physical properties were not affected by moisture although the off-axis properties of unmodified and modified matrix decreased by 52 and 66% on moisture absorption, which proved that moisture hampers the matrix properties. Also, while the effect of moisture was not at all noticeable on carbon fiber/PEEK laminate, 15% of its effect was observed on carbon fiber/modified epoxy laminate and 7% on carbon fiber/epoxy laminate.

Haddar et al. [87] worked on the effect of hygrothermal ageing on the monotonic and cyclic loadings of the glass fiber reinforced polyamide with fiber fraction of 50%. The testing samples were immersed in distilled water and salt solution (5g/l NaCl aq.) at 90°C to increase moisture infusion. It was detected that with an increase in immersion time, the moisture absorption rate and the extent of damage increased because water molecules have a tendency to break secondary bond between the polar groups. This, in turn, hampers mechanical cohesion and stiffness of the material. Addition of humidity caused swelling and plasticization in the samples, which could be attributed to the increment of the mass and decrement of properties in the samples. Also, samples aged under both the fluids (distilled water and salt solution) showed ductile fracture which could again be attributed to secondary bond breakage. Fatigue tests were carried out at room temperature for both the aged and the non-aged specimens. The S–N curve for the aged and the unaged specimens appeared different in slope and position. Again, fatigue tests showed degraded life of the aged samples due to the weakening of matrix. This resulted in the

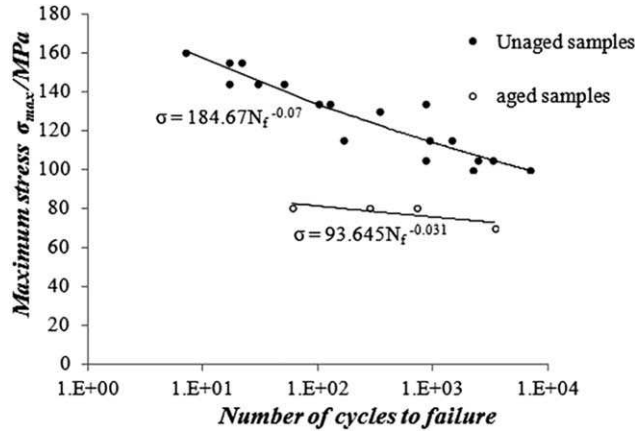

FIG. 36. Wohler curve for aged and unaged samples [87].

failure of samples by fiber breakage and/or pullout. The pulled out fibers were cleaner showing a degraded matrix-fiber interface. Figure 36 presents a comparative study of both the specimens. The decline in the curve was quantified by following equation:

$$\sigma_{max} = \sigma_f N_f^b \quad (14)$$

where σ_f is the fatigue strength coefficient and b is the fatigue strength exponent.

SUMMARY

Nowadays carbon fiber and glass fiber reinforced composites are being increasingly used in different fields of engineering by replacing conventional materials. Advantages of these composite materials over conventional materials include higher stiffness, higher strength, better fatigue behavior, corrosion resistance, and tailored properties. Conversely, delamination, discontinuous stress, reparability, and interchangeability are the disadvantages of polymer composites. Fatigue behavior of composite materials is different from that of the metals. Composites are inhomogeneous and anisotropic as compared to metals which are homogenous in nature and isotropic in behavior. In fatigue, composite materials undergo a series of changes, that is, matrix cracking, fiber-matrix debonding, fiber breaking and finally the failure. Thus, matrix, fiber and interface between fibers and materials play an important role in deciding the fatigue behavior of a laminate.

Due to their brittle nature, the polymer-based composites fail at low strains, thus, making it difficult to work on the stress-controlled fatigue. For a woven fabric, reinforced polymer composites both in warp and weft directions are equally important. Use of these fabrics increases the strength in depth. However, a common problem associated with these materials is the formation of resin-rich region. Failure occurs at these spaces, thus initiating failure even at a lower number of cycles. Addition of CNTs in the matrix increases the static strength of the material. It also enhances the fatigue life as load bearing capacity of the laminate increases. One can observe that addition of CNTs to modify the damage mechanism of the composite in the fatigue test shifts the damage zones to the right side. In the process, it is proved that with the inclusion of CNTs, each phase of damage increases for a certain number of cycles, increasing, in turn, the total number of cycles.

An increase in fiber volume fraction increases the fatigue performance of the composite. Stacking sequence has its own effect on the cyclic loading. As the strain remains the same, in each lamina stress varies according to the ply direction. Thus, ply with higher stress fails earlier as compared to the ply with lower stress. The mean stress has significant effect on the fatigue properties of the composite. With the mean stress defining the stress ratio or vice versa, by increasing the stress ratio, the fatigue life of the composite can be reduced. Moreover, testing frequency hampers the fatigue performance of the composite. Polymer-based composites, which is viscoelastic in nature, are sensitive to temperatures as the glass transition temperature (T_g) changes the properties of the polymer. At this temperature, the glassy appearing brittle material becomes soft and rubbery, thus losing all or some of its stiffness. The higher the frequency, the sooner the sample will reach its glass transition temperature (T_g).

The hysteresis curves of the composite materials are not persistent like metals. Following the failure, these curves tend to move toward higher strain, which indicates occurrence of failure at the phase. The area bound by the hysteresis curve shows loss of stiffness, which gets better by the addition of CNTs. This increases the number of fatigue cycles. Stress concentration or notch lowers the fatigue life of a composite. It also defines the area from where failure will initiate. As the temperature increases, the effect of stress concentration minimizes. The use of end tabs as suggested in ASTM D3479M also causes stress concentration but it also reduces the chances of failure within the grips. Multi axial stress is common as no material is flawless. Addition of CNTs causes applied stress to become multi-axial. With increase in biaxiality ratio, the fatigue failure takes place earlier.

Temperature has its own effect on the fatigue life of polymer-based composites. At elevated temperatures, material fails earlier. Conversely, at lower or cryogenic temperatures, fatigue strength and life of the material increase. Addition of CNTs reduces the cryogenic fatigue properties of the composite. Moisture in glass fiber-based composites degrades the fatigue properties. Fiber swelling, interface weakening, matrix corrosion are common in such case. Conversely, carbon fiber-based composites show nominal deviation in the properties. Thus, in general, addition of CNTs increases the fatigue performance of the composites as carbon fibers possess better fatigue properties as compared to glass fibers either at room temperature or at an increased temperature along with nominal effect of moisture.

NOMENCLATURE

V_f	fiber volume fraction
N_f	Number of cycles to failure
K	Slope of the intercept on S–N curve
σ_a	Amplitude of alternating stress
σ_T	Tensile strength
σ_a^χ	Alternating stress at critical stress ratio
ψ_χ	Fatigue strength ratio for cyclic loading at critical stress ratio
R	Stress ratio
σ_u	Ultimate strength
σ_m	Mean stress
χ	Critical stress ratio
σ_c	Compressive strength
σ_m^χ	Mean stress at critical stress ratio
σ_B	Reference strength
σ_{max}^x	Maximum stress at critical R

 DOI 10.1002/pc

REFERENCES

1. A.R. Offringa, Thermoplastic composites-Rapid processing applications, in 41st ICAC, Nottingham 161 (1995).
2. G. Marsh, *Mater. Today*, **6**, 36 (2003).
3. A.P. Mouritz, E. Geuert, P. Burchill, and K. Challis, *Compos. Struct.*, **53**, 21 (2001).
4. P. Brondsted, H. Lilholt, and A. Lystrup, *Annu. Rev. Mater. Res.*, **35**, 505 (2005).
5. G. Moritis, *Oil Gas J.*, **101**, 54 (2003).
6. P.K. Mallick, *Fibre reinforced composites: Materials and Design*, Florida (1993).
7. M. Biron, Thermoplastics and thermoplastic composites, *Massachusetts* (2013).
8. D. Hull and T.W. Clyne, *Cambridge Solid State Science Series*, (1996).
9. S. Iijima, *Nature*, 56 (1991).
10. E.W. Wong, P.E. Sheen, and C.M. Lieber, *Science*, **277**, 1971 (1997).
11. K.T. Lau and D. Hui, *Compos. Part B Eng.*, **33**, 263 (2002).
12. S. Iijima, C. Brabec, A. Maiti, and J. Bernhole, *J. Chem. Phys.*, **104**, 2089 (1996).
13. W. Zou, Z.-J. Du, Y.-X. Liu, X. Yang, H.Q. Li, and C. Zhang, *Compos. Sci. Technol.*, **68**, 3259 (2008).
14. B. Harris. "Fatigue in Composites," in *Science and Technology of the Fatigue Response of Fibre Reinforced Plastics*, Florida, (2003).
15. K.L. Reifsnider and A. Talug, *Int. J. Fatigue*, **2**, 3 (1980).
16. B.D. Agarwal and J.W. Dally, *J. Mater. Sci.*, **10**, 193 (1975).
17. J. Brunbauer and G. Pinter, *Int. J. Fatigue*, **75**, 28 (2015).
18. W. Zhang, Z. Zhou, B. Zhang, and S. Zhao, *Mater. Des.*, **66**, 3259 (2015).
19. W.F. Hosford, Elementary Materials Science, ASM International Ohio (USA) 44073-0002 (2013).
20. J.B. Knoll, B.T. Riecken, N. Kosmann, S. Chandrasekaran, K. Schulte, and B. Fiedler, *Compos. Part A*, **67**, 233 (2014).
21. L. Böger, J. Sumfleth, H. Hedemann, and K. Schulte, *Compos. Part A*, **41**, 1419 (2010).
22. Z. Wu, X. Wang, K. Iwashita, T. Sasaki, and Y. Hamaguchi, *Compos. Part B*, **41**, 396 (2010).
23. L.P. Borrego, J.D.M. Costa, J.A.M. Ferreira, and H. Silva, *Compos. Part B*, **62**, 67 (2014).
24. T. Takeda, W. Fan, Q.-P. Feng, S.-Y. Fu, F. Narita, and Y. Shindo, *Cryogenics*, **58**, 33 (2013).
25. C.R. Kennedy, C.M. Brádaigh, and S.B. Leen, *Compos. Struct.*, **106**, 201 (2013).
26. O.J. Nixon-Pearson, S.R. Hallett, P.J. Withers, and J. Rouse, *Compos. Struct.*, **106**, 882 (2013).
27. M. Gude, W. Hufenbach, I. Koch, R. Koschichow, K. Schulte, and J. Knoll, *Proc. Mater. Sci.*, **2**, 18 (2013).
28. B. Esmaeillou, P. Ferreira, V. Bellenger, and A. Tcharkhtchi, *Polym. Compos.*, **33**, 540 (2012).
29. A. Vavouliotis, A. Paipetis, and V. Kostopoulos, *Compos. Sci. Technol.*, **71**, 630 (2011).
30. I.D. Baere, W.V. Paepegem, M. Quaresimin, and J. Degrieck, *Polym. Test.*, **30**, 625 (2011).
31. M. Bizuel, C. Bouvet, J.J. Barrau, and R. Cuenca, *Compos. Sci. Technol.*, **71**, 289 (2011).
32. A. Hosoi, K. Takamura, N. Sato, and H. Kawada, *Int. J. Fatigue*, **33**, 781 (2011).
33. M. Bizuel, C. Bouvet, J.J. Barrau, and R. Cuence, *Int. J. Fatigue*, **32**, 60 (2010).
34. A. Goel, K.K. Chawla, U.K. Vaidya, N. Chawla, and M. Koopman, *Mater. Charact.*, **60**, 537 (2009).
35. A. Hosoi, Y. Arao, and H. Kawada, *Compos. Sci. Technol.*, **69**, 1388 (2009).
36. E.C. Botelho, M.C. Rezende, S. Mayer, and H. Voorwald, *J. Mater. Sci.*, **43**, 3166 (2008).
37. C.S. Grimmer and C.K.H. Dharan, *J. Mater. Sci.*, **43**, 4487 (2008).
38. M.P. Cavatorta, *J. Mater. Sci.*, **42**, 8636 (2007).
39. M. Kawai and M. Koizumi, *Compos. Part A*, **38**, 2342 (2007).
40. Y. Shindo, S. Takano, K. Horiguchi, and T. Sato, *Cryogenics*, **46**, 794 (2006).
41. S. Kumagai, Y. Shindo, and A. Inamoto, *Cryogenics*, **45**, 123 (2005).
42. M.N. Bureau and J. Denault, *Polym. Compos.*, **25**, 622 (2004).
43. S.D. Pandita and I. Verpoest, *Compos. Struct.*, **64**, 199 (2004).
44. J. Gassan and T. Dietz, *J. Mater. Sci.*, **8**, 2755 (2003).
45. J. Vina, M.A. Castrillo, A. Arguelles, and I. Vina, *Polym. Compos.*, **23**, 619 (2002).
46. T. Yokozeki, T. Aoki, and T. Ishikawa, *Compos. Sci. Technol.*, **62**, 1223 (2002).
47. J. Tong, *Int. J. Fatigue*, **24**, 219 (2002).
48. V. Barron, M. Buggy, and N.H. McKenna, *J. Mater. Sci.*, **36**, 1755 (2001).
49. S.D. Pandita, G. Huysmans, M. Wevers, and I. Verpoest, *Compos. Part A*, **32**, 1533 (2001).
50. S. Ogihara, N. Takeda, S. Kobayashi, and A. Kobayashi, *Compos. Sci. Technol.*, **59**, 1387 (1999).
51. N. Takeda, S. Kobayashi, S. Ogihara, and A. Kobayashi, *Int. J. Fatigue*, **21**, 235 (1999).
52. H.A. Whitworth, *Compos. Struct.*, **40**, 2 142 (1998).
53. C.E. Demers, *Constr. Build. Mater.*, **12**, 303 (1998).
54. X. Wang and D.D.L. Chung, *Polym. Compos.*, **18**, 692 (1997).
55. C.C.M. Ma, S.H. Lin, N.H. Tai, S.H. Wu, and J.F. Wu, *Polym. Compos.*, **16**, 215 (1995).
56. K.L. Reifsnider, K. Schulte, and J.C. Duke, ASTM STP 813, 136 (1983).
57. P. Ladeveze and G. Lubineau, *Compos. Sci. Technol.*, **62**, 533 (2002).
58. M.J. Hinton, A.S. Kaddour, and P.D. Soden, *The World Wide Failure Exercise*, Elsevier, Kindlington, Oxford, OX5 1GB, UK. (2004).
59. D. Vasiukov, S. Panier, and A. Hachemi, *Int. J. Fatigue*, **70**, 289 (2015).
60. K.M. Mini, M. Lakshmanan, L. Mathew, and M. Mukundan, *FFEMS*, **35**, 1160 (2012).

61. D. Schütz and J.J. Gerharz, *Composites*, **8**, 245 (1977).
62. J. Montesano, Z. Fawaz, and H. Bougherara, *Compos. Struct.*, **97**, 76 (2013).
63. H.T. Hahn and R.Y. Kim, *J. Compos. Mater.*, **9**, 297 (1975).
64. L.J. Broutman and S. Sahu, "Composite Materials: Testing and Design," in 2nd Conference: ASTM International 170 (1972).
65. I.D. Baere, W.V. Paepegem, C. Hochard, and J. Degrieck, *Polym. Test.*, **30**, 663 (2011).
66. T.P. Philippidis and V.A. Passipoularidis, *Int. J. Fatigue*, **29**, 2104 (2007).
67. J.N. Yang, *J. Compos. Mater.*, **12**, 19 (1978).
68. J. Anderson and J. Korsgaard, *ICCM*, **2**, 135 (1997).
69. T.P. Philippidis, T.T. Assimukopoulou, A.E. Antoniou, and V.A. Passipoularidis, *OB-TGS-R008*, (2005).
70. W. Hwang and K.S. Han, *J. Compos. Mater.*, **2**, 154 (1986).
71. J. Brunbauer and G. Pinter, *Polym. Test.*, **40**, 256 (2014).
72. J.W. Mar and K.Y. Lin, *Struct. Compos. Mater.*, **14**, 703 (1977).
73. W.R. Broughton, M.R.L. Gower, M.J. Lodeiro, G.D. Pilkington, and R.M. Shaw, *Compos. Part A*, **42**, 1310 (2011).
74. B. Aidi, M.K. Philen, and S.W. Case, *Compos. Part A*, **74**, 47 (2015).
75. ASTM D3039/D3039M – 14. Standard Test Method for Tensile Properties of Polymer Matrix Composite Materials.
76. ASTM D3479/D3479M – 12. Standard Test Method for Tension-Tension Fatigue of Polymer Matrix Composite Materials
77. P.B.S. Bailey and A.D. Lafferty, *eXPRESS Polym. Lett.*, **9**, 480 (2015).
78. I.D. Baere, W.V. Paepegem, and J. Degrieck, *Polym. Compos.*, **38**, 381 (2009).
79. S. Amijima, T. Fujii, and M. Hamaguchi, *Composites*, **22**, 281 (1991).
80. H. Kawakami and T.J. Fujii, *J. Rein. Plast. Compos.*, **1996**, **15**, 183 (1996).
81. T. Fujii and T. Shiina, *J. Compos. Mater.*, **28**, 234 (1994).
82. M.-H.R. Jen, Y.-C. Tseng, H.-K. Kung, and J.C. Huang, *Compos. Part B*, **39**, 1142 (2008).
83. M. Kawai and T. Taniguchi, *Compos. Part A*, **37**, 243 (2006).
84. A. Rotem, and H. G. Nelson, NASA Technical Memorandum, 78538, 1 (1978)
85. Y. Hu, A.W. Lang, X. Li, and S.R. Nutt, *Polym. Degrad. Stab.*, **110**, 464 (2014).
86. R. Selzer and K. Friedrich, *Compos. Part: A*, **28**, 595 (1997).
87. N. Haddar, I. Ksouri, T. Kallel, and N. Mnif, *Polym. Compos.*, **35**, 501 (2014).

 DOI 10.1002/pc